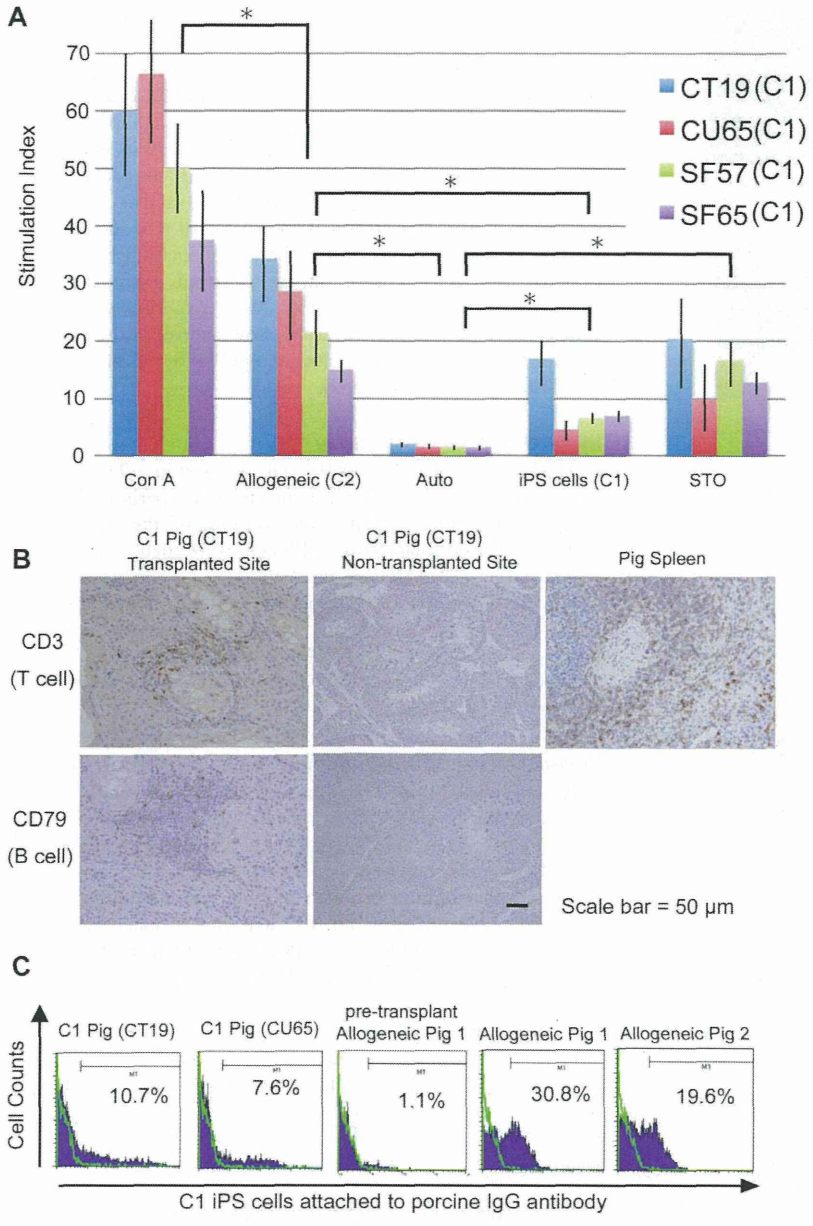

Figure 1. Cellular and humoral immune responses in an SLA-matched setting. (A) Mixed lymphocyte reactions (MLRs) against allogeneic (C2) porcine embryonic fibroblasts (PEFs), C1 iPS cells and STO feeder cells. Peripheral blood mononuclear cells (PBMCs) supplemented with concanavalin A (Con A) and C2 PEFs were used as positive controls, and autologous PBMCs (C1) were used as a negative control. The stimulation index of C1 iPS cells was significantly lower than that of allogeneic cells ($^{*}p<0.01$), but significantly higher than that of autologous cells ($^{*}p<0.01$). MLR was performed in triplicate and repeated three times and a typical result was shown. (B) Immunohistochemical staining with anti-CD3 and anti-CD79 antibodies. Pig spleen was stained with the anti-CD3 antibody as a positive control. Slight infiltration of CD3+ T-cells and CD79+ B cells was detected at the transplantation site in the SLA-matched pig CT19. (C) Porcine IgG antibodies against C1 iPS cells were determined by flow cytometry. As SLA-mismatched recipients, miniature pigs that were not C1 or C2 were used. The porcine IgG against C1 iPS cells was detected at much lower levels in the SLA-matched C1 pigs (CT19 and CU65) than in the SLA-mismatched allogeneic pigs. Cells labeled with secondary antibody without porcine serum as a negative control.
doi:10.1371/journal.pone.0098319.g001

Cell Sorter SH800 (SONY, Tokyo, Japan), the fraction of CD3-negative and CD16-positive cells was collected. The collected cells were used as porcine NK cells. C1 iPS cells were incubated as target cells with NK cells at ratios of 1:30 for 6 h at 38.5°C in DMEM supplemented with 1% FBS, 0.1 mM 2-mercaptoethanol and 1 ng/ml recombinant porcine IL-2 (R&D systems). The cytotoxicity of C1 iPS cells to NK cells was assessed by lactate dehydrogenase (LDH) release assay. Percent cytotoxicity was calculated as follows: cytotoxicity (%) = (Experimental value − Effector control − Target control) × 100/(High control − Target control). The High control was obtained after incubating C1 iPS cells with 2% Triton X-100. The Effector control and the Target

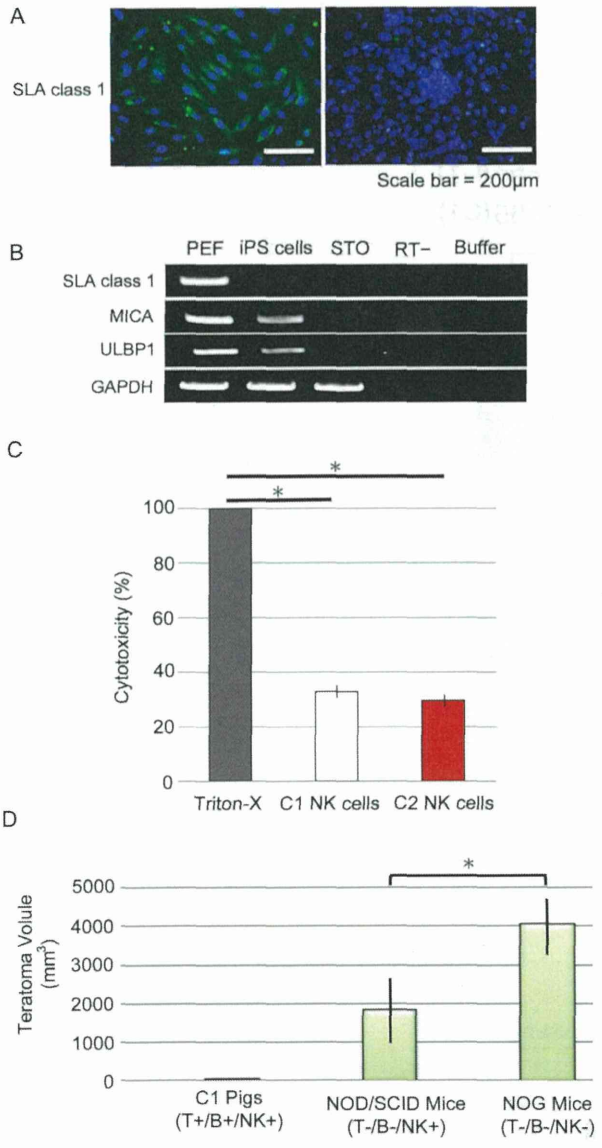

Figure 2. Susceptibility of C1 iPS cells to NK cells. (A) Immunocytochemical staining with an anti-porcine SLA class I antibody. Porcine PEFs showed positive staining for SLA class I, but C1 iPS cells were negative. (B) Reverse-transcription polymerase chain reaction (RT-PCR) analysis of the expression of *SLA class I* and ligands for NK cells. Lane 1, PEF; 2, C1 iPS cells; 3, STO feeder cells; 4, no reverse transcriptase; and 5, RT-PCR buffer alone. *MICA* and *ULBP1*, ligands for NK cells, were expressed on C1 iPS cells. *GAPDH* was used as a loading control. (C) Cell injury by NK cells was assessed by measuring LDH released in the supernatants as described in the Materials and Methods. Triton-X (2%) was used as a positive control. The percent cytotoxicity was quantified and shown as mean of triplicate. Two independent experiments were performed and similar results were obtained. (D) Estimated volumes of the teratomas in immunodeficient mice and SLA-matched pigs. C1 iPS cells were transplanted into NK-competent NOD/SCID ($n=14$) and NK-deficient NOG ($n=14$) mice, and C1 pigs ($n=5$). After transplantation of C1 iPS cells (1×10^6 cells/site) into immunodeficient mice, the teratomas were dissected and their size (diameter) was measured ($^*p<0.01$). After transplantation of C1 iPS cells (3×10^7 cells/site) into C1 pigs, no teratomas were observed.
doi:10.1371/journal.pone.0098319.g002

control were obtained after incubating NK cells alone and C1 iPS cells alone, respectively.

In vitro complement-mediated cytotoxicity assay

The cytotoxicity of C1 iPS cells to serum complement was assessed by LDH release assay. C1 iPS cells were incubated with C1 porcine serum that was heat–non-treated (complement–non-inactivated) at ratios of 3:100 to 30:100 for 30 min at 38.5°C. The supernatants were centrifuged at $250\times g$ for 10 min and examined for the release of LDH using the Cytotoxicity Detection Kit (Takara Bio Inc, Tokyo, Japan). Percent cytotoxicity was calculated as follows: cytotoxicity (%) = (Experimental value − Low control) × 100/(High control − Low control). Low and High controls were obtained after incubating C1 iPS cells alone or with 2% Triton X-100, respectively.

In vitro phagocytosis assay

PBMCs were plated at 5×10^4 cells per well in a 24-well tissue-culture plate at 38.5°C for 2 hours to allow peritoneal macrophages to attach to the plate. After washing off the non-adherent cells, 2×10^5 EGFP-labeled C1 iPS cells were then added to each well as target cells. After co-incubation of macrophages and iPS cells with or without CD47-blocking antibody (BRIC126, Santa Cruz; 1:50) for two hours, macrophages were stained with anti-porcine monocytes antibody (Antigenix America, USA; 1:100). Phagocytic index (PI) was calculated as the number of engulfed iPS cells per 100 iPS cells.

Reverse transcription-polymerase chain reaction (RT-PCR)

Reverse transcription reactions were performed using a Thermo Scientific Verso cDNA Synthesis kit (Thermo) with random hexamer primers. PCR was performed with Ex-Taq (Takara Bio Inc). PCR products were separated on 2% agarose gel and visualized by ethidium bromide staining. Semi-quantitative RT-PCR was performed using an ABI Step One (Applied Biosystems, CA, USA) with SYBR green PCR mix (Qiagen, CA, USA). Primer sequences are listed in Table S1.

Statistical analysis

Data are expressed as mean ± standard deviation. The significance of differences between groups was tested using Student's *t*-test.

Results

Cellular and humoral immune responses in an SLA-matched setting

First, we transplanted porcine iPS cells derived from the C1 strain of Clawn miniature swine [24] into immunodeficient mice, and confirmed formation of teratomas from C1 iPS cells (Fig. S1 in File S1). Next, we tried to develop teratomas in pigs. Pigs were treated with immunosuppressants (tacrolimus, mycophenolate mofetil and steroid). Within 1–2 months after administration, they suffered from severe infection such as mediastinitis and reached the end-point when they should be euthanized. Thus, it is technically and ethically difficult to maintain such pigs until transplanted iPS cells develop teratomas. Then, we transplanted C1 iPS cells (3×10^7 cells/site) into the testes ($n=4$) or ovary ($n=1$) of SLA-matched swine (i.e., C1-to-C1) without immunosuppression (Fig. S2 in File S1). C1 iPS cells were also transplanted into the ovary ($n=1$) of an SLA-mismatched C2 female pig (i.e., C1-to-C2) without immunosuppression. No teratomas developed in any of the recipients tested on days 47 to 125 after transplantation.

Table 1. The teratoma formation in SLA-matched pigs and immunodeficient mice following injection of C1 iPS cells.

Recipients	SLA-matched pigs (T+/B+/NK+)	NOD/SCID mice (T-/B-/NK+)	NOG mice (T-/B-/NK−)	NOG mice injected with iPS cells cultured with serum-complement)
Number of teratoma formation per total	0/5	8/14	11/14	0/6
Frequency (%)	0	57.1	78.6	0

doi:10.1371/journal.pone.0098319.t001

Mixed lymphocyte reaction (MLR) assays showed that the T-cell response to SLA-matched C1 iPS cells was indeed attenuated compared to SLA-mismatched C2 cells (Fig. 1A), but still stronger than to autologous cells. Notably, the T-cell reactivity of CT19 pig was higher compared to other recipients (Fig. 1A). This particular recipient showed in vivo evidence of inflammation and infiltration of a few CD3+ T cells and CD79+ B cells at the transplanted site (Fig. 1B). In addition, we performed ELISA to detect IFN-γ in the porcine serum. Although serum IFN-γ was clearly detected in the SLA-mismatched setting (C1-to-C2), it was undetectable in the SLA-matched setting (C1-to-C1) (Fig. S3 in File S1).

With regard to humoral immune responses, IgG against C1 iPS cells was detected in SLA-matched recipient pigs at day 17 or 19 after transplantation, but the level of IgG was lower than that in SLA-unmatched recipient pigs (Fig. 1C). Thus, matching of SLA could also attenuate the humoral immune response. Taken together, both cellular and humoral immune responses would be attenuated due to the matching of SLA.

Involvement of natural killer (NK) cells in rejection of C1 iPS cells in vivo

We then examined innate immune responses. C1 iPS cells express no or very low levels of SLA class I molecules [24] (Fig. 2A). Therefore, the injected C1 iPS cells are likely targets of NK cells, which kill MHC class I-negative cells [25]. In addition, our RT-PCR analysis demonstrated that C1 iPS cells expressed both MHC class I-related chain A (*MICA*) and UL16-binding protein 1 (*ULBP1*) (Fig. 2B). Previous reports demonstrated that pluripotent stem cells, such as ES cells, iPS cells, and germ-line stem cells are highly susceptible to NK cells because they express ligands for NK cells, such as *MICA* and *ULBP1* [26,27]. The absence of SLA class I expression and the presence of NK ligands on C1 iPS cells suggest that they are susceptible to NK cells.

Therefore, we performed a cytotoxicity assay to examine whether porcine NK cells kill C1 iPS cells in vitro. As shown in Figure 2C, C1 iPS cells released LDH after incubation with even the SLA-matched NK cells, as well as the SLA-mismatched NK cells (Fig. 2C). This result indicates that C1 iPS cells are killed by NK cells. To examine whether the growth of C1 iPS cells are affected by NK cells in vivo, we transplanted 1×10^6 C1 iPS cells/site intramuscularly into NK-competent NOD/SCID (T-B- NK+) mice and NK-deficient NOG (T- B- NK-) mice (Table 1). We found that the sizes of the teratomas that developed in NK-deficient NOG mice ($n=10$) were significantly larger than those that developed in the NK-competent NOD/SCID mice ($n=8$) ($p<0.01$) (Fig. 2D). These observations suggest that the overall growth of C1 iPS cells is hampered by NK cells in vivo.

Susceptibility of C1 iPS cells to complement-mediated cytotoxicity

It has been reported that mouse ES cells and mesenchymal stem cells are sensitive to serum complement [28,29]. Complement activity is regulated indirectly by sialic acids on the cell surface [30]. We found that C1 iPS cells did not express sialic acids (Fig. 3A), suggesting that the cells are sensitive to complement. To assess whether C1 iPS cells were susceptible to complement, the cells were incubated with heat–non-treated (complement–non-inactivated) porcine serum. We found that C1 iPS cells released significant amounts of LDH after incubation with the C1 porcine serum, indicating that C1 iPS cells were injured by complement (Fig. 3B).

We examined whether complement hamper the formation of teratomas in vivo. C1 iPS cells were cultured with the porcine serum for 6 hours; then 1×10^6 cells/site were transplanted into NOG mice ($n=6$). No teratomas developed in any of the mice at 2 months after transplantation (Table 1) in agreement with a previous report [28]. These results indicate that C1 iPS cells are susceptible to complement-mediated injury.

Possible control of macrophage phagocytosis by CD47 ligand on C1 iPS cells

We examined whether C1 iPS cells are susceptible to macrophage phagocytosis. Macrophage phagocytosis is regulated negatively by interaction of a CD47 ligand ("don't-eat-me" signal) and an immune inhibitory receptor on the macrophage [31,32,33,34]. Semi-quantitative real-time PCR and immunocytochemistry revealed that the C1 iPS cells expressed CD47 to the same extent as fibroblasts (Fig. 4A), suggesting that C1 iPS cells evade macrophage phagocytosis in the C1 recipients.

Therefore, we performed a phagocytosis assay to examine whether C1 iPS cells evade macrophages in vitro. We found that phagocytosis index (PI) was $33.7\pm1.5\%$; only one third of iPS cells were engulfed by macrophages (Fig. 4B). On the other hand, significantly more of iPS cells were subjected to phagocytosis ($PI=63.4\pm2.8\%$, $p<0.01$) when the cells were incubated with anti-CD47 antibodies (Fig. 4B). These results clearly indicate that engulfment of iPS cells by macrophages is promoted by blocking CD47, suggesting that iPS cells evade macrophagic phagocytosis through the CD47 ligand.

Discussion

In this study, we investigated immune responses following transplantation of porcine iPS cells into SLA-matched recipients. Our results indicate that SLA-matched iPS cells elicit significantly less cellular and humoral immune responses but they still elicit potent innate immune responses, possibly resulting in the failure in the formation of teratomas. We suggested that innate immunity including serum complement play a role in the in vivo clearance of

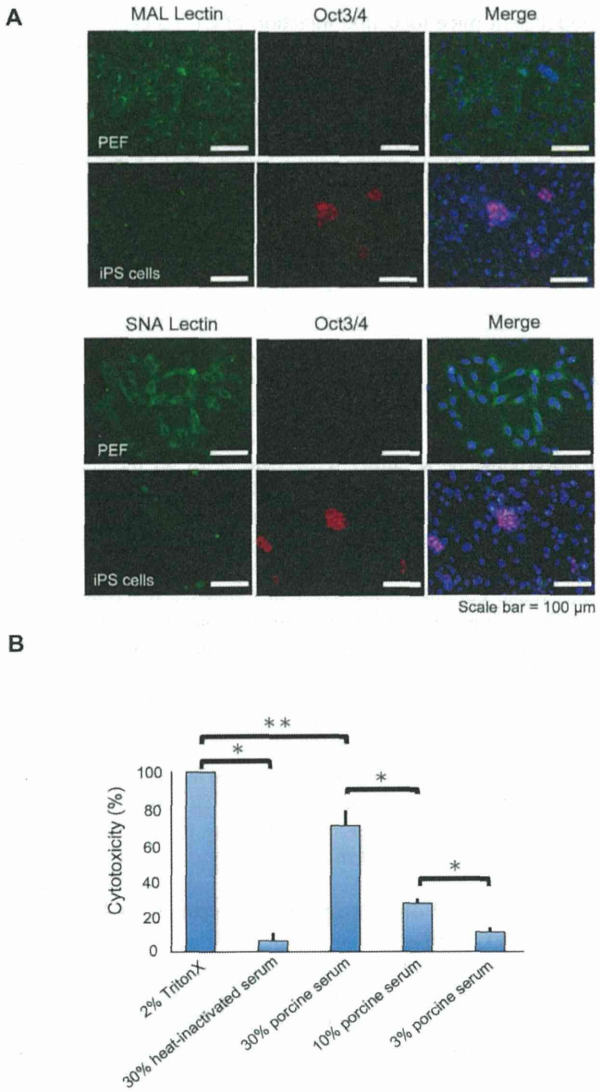

Figure 3. Complement-mediated cytotoxicity to C1 iPS cells. (A) *Cytochemical assay for sialic acids using lectins. The expression of sialic* acids was examined with SNA lectin and MAL lectin, both of which specifically bind to sialic acids. C1 iPS cells exhibited very low levels of sialic acids compared to fibroblasts. C1 iPS cells, but not PEFs, expressed Oct3/4. (B) Cell injury by complement was assessed by measuring LDH released in the supernatants described in the Materials and Methods. Triton-X (2%) was used as a positive control, and 30% of heat-inactivated (complement-inactivated) serum was used as a negative control. The percent cytotoxicity was indicated as average values of triplicate ($^{*}p<0.01$, $^{**}p<0.05$). Three independent experiments were conducted and similar results were obtained.
doi:10.1371/journal.pone.0098319.g003

C1 iPS cells. Several studies have reported that pluripotent stem cells are susceptible to NK cells and serum complement, and that this susceptibility results in the failure to form teratomas in immunodeficient mice [27,28,35]. Here, we have shown that it is also the case in the porcine SLA-matched transplantation setting (Table 1).

Our analyses also suggest that macrophages were unlikely to be involved in the rejection of SLA-matched iPS cells. Although C1 iPS cells do not possess SLA class I (Fig. 2A, B) or sialic acids (Fig. 3A), the cells did express CD47 as a marker of self (Fig. 4A). A similar situation occurs in murine red blood cells and in hematopoietic stem cells, which express CD47 that prevents macrophage phagocytosis [31,33]. The PI values of 33.7±1.5% obtained in this study were low enough to say that C1 iPS cells evade phagocytosis.

The values increased to 63.4±2.8% with the CD47-blocking antibody (Fig. 4B). It is therefore likely that C1 iPS cells evade phagocytosis by macrophages through CD47, also considering other published reports together [32,34]. For example, PI of pig lymphoblastoid cells with human macrophages was about 25% when CD47 was present, although it was about 65% when CD47 was absent [32]. In the other report, PI of human myeloma cells with mouse macrophages was about 50% when CD47 is present, but it increases to about 70% when CD47 was absent [34].

The T-cell response to porcine iPS cells was attenuated in the SLA-matched allogeneic transplantation setting compared to the SLA-mismatched setting, but still stronger than that to autologous cells (Fig. 1A). There are three possible reasons to explain the remaining cellular and humoral immune responses in the SLA-matched setting. First, unlike strictly matched mouse syngeneic settings, there are a few mismatches in SLA or mitochondrial DNA or other unknown minor antigens between donor iPS cells and recipients [36]. These mismatches may trigger immune responses. In addition, immune reactions can be elicited by sex-mismatches between donors and recipients. Minor histocompatibility antigen in a Y chromosome is immunogenic in a female, although this particular mismatch is unlikely because C1 iPS cells are derived from a female.

Second, the xenogeneic transgenes used to induce pluripotency might induce the immune response to C1 iPS cells. Exogenous "Yamanaka factors" (ectopically expressed *OCT3/4*, *SOX2*, *KLF4* and *c-MYC*) used in the present study are derived from human genes and are thus potentially immunogenic in pigs (Fig. S4 in File S1), although this is not clinically relevant. In addition, a previous study showed that Oct3/4 antigens, even allogeneic ones, are immunogenic and that cells expressing *OCT3/4* become targets of cytotoxic T lymphocytes [37]. C1 iPS cells that retained or reactivated expression of the xenogeneic transgenes might have elicited immunoreactions in the C1 pigs.

Third, STO feeder cells are murine cells and immunogenic in pigs (Fig. 1A). Some STO feeder cells were present in the donor cells (Fig. S5 in File S1), and they may have induced cellular immune responses. Although feeder cells may be excluded with a cell sorter, trypsinizing ES or iPS cells into single cells hampers their ability to develop teratomas [35]. In addition, we transplanted a large number of pig iPS cells (more than 10^7 in 30–50 dishes at once) into a pig. It is not realistic to prepare such a large number of cells with a cell sorter. In order to completely exclude feeder cells, iPS cells should be expanded under feeder-free conditions. It is certainly an important technique to be developed.

Concerning non-pluripotent stem cells, HLA-matched allogeneic transplantation of hematopoietic stem cells has been successfully conducted for the treatment of hematopoietic malignancies and solid tumors. The cells usually engraft with minimal conditioning of patients [38,39]. Therefore, it is unlikely that potent natural immunity will occur to hematopoietic stem cells after transplantation. The occurrence of potent immunity seems quite specific to pluripotent stem cells such as iPS cells. It is no wonder, considering that iPS cells lack the expression of MHC class I and sialic acids, eliciting natural immune responses. Other tissue stem cells including hematopoietic stem cells, however, express both of them. That would be a great advantage for clinical applications of iPS cells, because iPS-derived differentiated cells

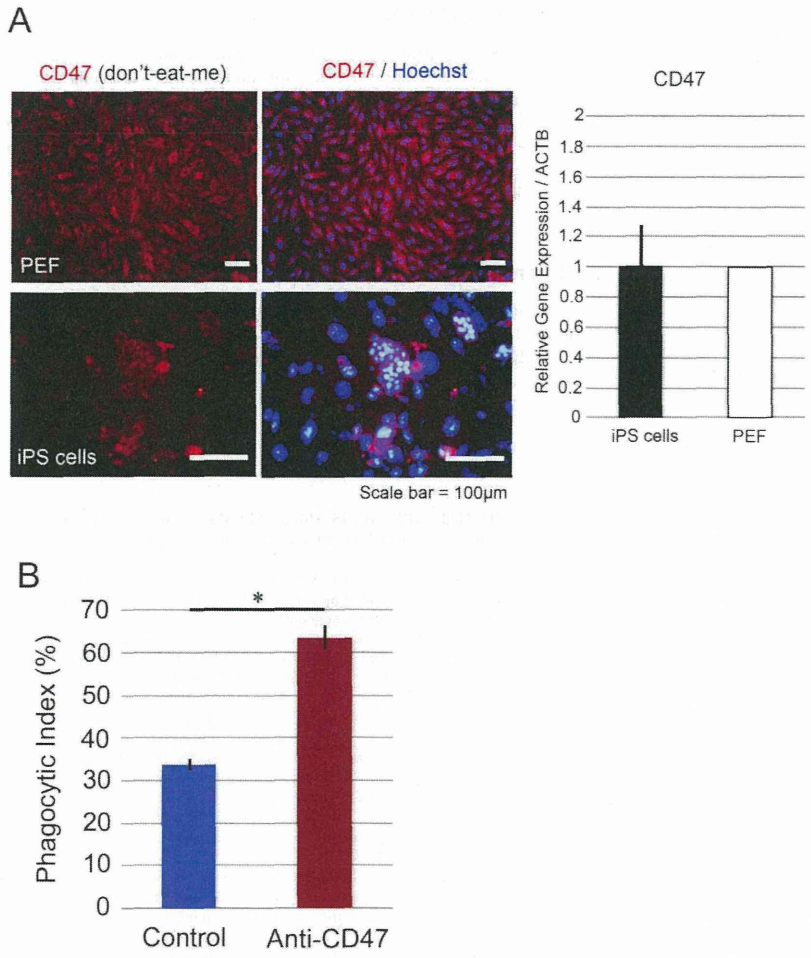

Figure 4. C1 iPS cells evade phagocytosis by macrophages through CD47 ligand. (A) Expression of CD47 was evaluated by immunocytochemistry and semi-quantitative PCR ($n=3$). C1 iPS cells expressed CD47 to the same extent as fibroblasts. (B) Phagocytosis index (PI) was the number of iPS cells phagocytosed per 100 iPS cells, and it was 33.7±1.5%. The anti-CD47 antibody was then used to block the binding of CD47 to SIRPα. The PI value increased to 63.4±2.8%, showing that CD47 is responsible for the escape of iPS cells from phagocytosis by macrophages ($^{*}p<0.01$).
doi:10.1371/journal.pone.0098319.g004

would engraft in recipients but undifferentiated iPS cells contaminated in grafts would be cleared by natural immune responses after transplantation. Whether it is the case is a next step to be examined in the SLA-defined transplantation model.

By extrapolation from our results using the SLA-matched setting, immune responses against undifferentiated human iPS cells will occur in the HLA-matched setting. To our knowledge, this is the first study to assess immune responses to iPS cells in an MHC-matched setting through use of inbred SLA-defined miniature swine.

Supporting Information

File S1 Contains the following files: **Figure S1.** Characterization of C1 iPS cells. (A) Immunocytochemical staining of C1 iPS cells for Oct3/4, Sox2, Nanog, and Stella. C1 iPS cells were also positive for AP activity. (B) Hematoxylin and eosin staining of teratomas derived from C1 iPS cells showing differentiation into all three germ layers, including stratified squamous epithelia (ectoderm) (a), bundles of nerve fibers (ectoderm) (b), muscle fibers (mesoderm) (c), and columnar epithelia (endoderm) (d). (C) Immunocytochemical staining of differentiated C1 iPS cells in vitro. These cells were positive for GFAP, Tuj-1, Vimentin, FOXA2, AFP, Nestin, Desmin, α-SMA, CK18 or Albumin. **Figure S2.** Transplantation of C1 iPS cells into porcine testes and ovaries. (A) Testes of C1 recipient pigs (a). Injection of C1 iPS cells into the testis using an ultrasound method (b). The yellow ellipse indicates the injection needle (c). (B) Injection of C1 iPS cells into the ovary after laparotomy (a). The transplanted side was labeled using string (b). The ovary on the non-transplanted side (c). (C) Genealogy of C1 Clawn miniature swine used in this study. The donor of the iPS cells was pig AT25. The SLA-matched recipients were pig CT19, CQ38, CU65, SF65 and SD57. Pig CQ74 was used as an SLA-mismatched recipient. The C1 strain was carefully maintained and the C1 status was confirmed by PCR (indicated by *). Pig CQ74 was unexpectedly C2 (indicated by **). The real parent pig P was considered to be C2. **Figure S3.** Serum concentrations of IFN-γ in pigs. Serum concentrations of IFN-γ were measured by ELISA. C1 PBMCs co-cultured with C2 PBMCs were used as a positive control. Serum IFN-γ was undetectable in the SLA-matched C1 recipients, although it was

clearly detectable in the SLA-mismatched setting. Two independent experiments were conducted in triplicate and similar results were obtained, one of which was shown here. Each data point represents the mean ± SEM. **Figure S4.** Sustained expression of the transgenes in C1 iPS cells and teratomas. Expression of the exogenous Yamanaka factors was evaluated by RT-PCR. The transgenes were derived from human genes. The primers for RT-PCR were designed to detect the specific retroviral sequences. β-actin was used as a loading control. **Figure S5.** Feeder cells present in donor cells. Flow cytometric analysis showed that feeder cells were present in donor cells. EGFP-labeled C1 iPS cells were used to distinguish from mouse feeder cells (STO). C1 iPS cells were harvested by trypsinization and then incubated on gelatin-coated dishes for 15 min to remove feeder cells. 27.4% of the harvested cells were feeder cells. **Table S1.** Primer sets used in the present study.
(DOC)

Acknowledgments

We thank Rikiya Ishino, Yutaka Furukawa, Tohru Wakui, Osamu Matsumoto, and Kazushi Miyazaki for their helpful assistance in cell transplantation (Jichi Medical University). We also thank Junichi Tottori for his helpful assistance in cell transplantation (Japan Farm). We appreciate Shigeo Masuda for his helpful advice and valuable discussion (Jichi Medical University). We are grateful to Sachi Okabayashi and Chieko Ohno for their technical supports (Tsukuba Primate Research Center).

Author Contributions

Conceived and designed the experiments: Y. Mizukami TA YH. Performed the experiments: Y. Mizukami TA HS Y. Makimura KY SH EK. Analyzed the data: Y. Mizukami TA YH. Contributed reagents/materials/analysis tools: HS SF. Wrote the paper: Y. Mizukami YH.

References

1. Takahashi K, Yamanaka S (2006) Induction of pluripotent stem cells from mouse embryonic and adult fibroblast cultures by defined factors. Cell 126: 663–676.
2. Takahashi K, Tanabe K, Ohnuki M, Narita M, Ichisaka T, et al (2007) Induction of pluripotent stem cells from adult human fibroblasts by defined factors. Cell 131: 861–872.
3. Hayashi K, Ogushi S, Kurimoto K, Shimamoto S, Ohta H, et al (2012) Offspring from oocytes derived from in vitro primordial germ cell-like cells in mice. Science 338: 971–975.
4. Yanagimachi MD, Niwa A, Tanaka T, Honda-Ozaki F, Nishimoto S, et al (2013) Robust and Highly-Efficient Differentiation of Functional Monocytic Cells from Human Pluripotent Stem Cells under Serum- and Feeder Cell-Free Conditions. PLoS One 4: e59243.
5. Yamaguchi T, Tashiro K, Tanaka S, Katayama S, Ishida W, et al (2013) Two-step differentiation of mast cells from induced pluripotent stem cells. Stem Cells Dev 22: 726–734.
6. Hanna J, Wernig M, Markoulaki S, Sun CW, Meissner A, et al (2007) Treatment of sickle cell anemia mouse model with iPS cells generated from autologous skin. Science 318: 1920–1923.
7. Alipio Z, Liao W, Roemer J, Waner M, Fink M, et al (2010) Reversal of hyperglycemia in diabetic mouse models using induced-pluripotent stem (iPS)-derived pancreatic beta-like cells. Proc Natl Acad Sci USA 107: 13426–13431.
8. Araki R, Uda M, Hoki Y, Sunayama M, Nakamura M, et al (2013) Negligible immunogenicity of terminally differentiated cells derived from induced pluripotent or embryonic stem cells. Nature 494: 100–104.
9. Guha P, Morgan JW, Mostoslavsky G, Rodrigues NP, Boyd AS (2013) Lack of Immune Response to Differentiated Cells Derived from Syngeneic Induced Pluripotent Stem Cells. Cell Stem Cell 12: 407–412.
10. Emborg ME, Liu Y, Xi J, Zhang X, Yin Y, et al (2013) Induced pluripotent stem cell-derived neural cells survive and mature in the nonhuman primate brain. Cell Reports 3: 646–650.
11. Morizane A, Doi D, Kikuchi T, Okita T, Hotta A, et al (2013) Direct Comparison of Autologous and Allogeneic Transplantation of iPSC-Derived Neural Cells in the Brain of a Nonhuman Primate. Stem Cell Reports 1: 283–292.
12. Kaneko S, Yamanaka S (2013) To Be Immunogenic, or Not to Be: That's the iPSC Question. Cell Stem Cell 12: 385–386.
13. Nakatsuji N, Nakajima F, Tokunaga K (2008) HLA-haplotype banking and iPS cells. Nat Biotechnol 7: 739–740.
14. Okita K, Matsumura Y, Sato Y, Okada A, Morizane A, et al (2011) A more efficient method to generate integration-free human iPS cells. Nature Methods 5: 409–412.
15. Taylor CJ, Peacock S, Chaudhry AN, Bradley JA, Bolton EM (2012) Generating an iPSC bank for HLA-matched tissue transplantation based on known donor and recipient HLA types. Cell Stem Cell 11: 147–152.
16. Zimmermann A, Preynat-Seauve O, Tiercy JM, Krause KH, Villard J (2012) Haplotype-based banking of human pluripotent stem cells for transplantation: potential and limitations. Stem Cells Dev 13: 2364–2673.
17. Sachs DH, Leight G, Cone J, Schwarz S, Stuart L, et al (1976) Transplantation in miniature swine. 1. Fixation of the major histocompatibility complex. Transplantation 22: 559–567.
18. Sachs DH (1994) The pig as a potential xenograft donor. Pathol Biol 42: 217–219.
19. Bollen P, Ellegaard L (1997) The Gottingen minipig in pharmacology and toxicology. Pharmacol Toxicol 80: 3–4.
20. Nakanishi Y, Ogawa K, Yanagita K (1991) Body measurement and some characteristics of inbred Clawn miniature pigs. Jpn J Swine Sci 28: 211.
21. Mezrich JD, Haller GW, Arn JS, Houser SL, Madsen JC (2003) Histocompatible miniature swine: an inbred large-animal model. Transplantation 75: 904–907.
22. Ando A, Kawata H, Shigenari A, Anzai T, Ota M, et al (2003) Genetic polymorphism of the swine major histocompatibility complex (SLA) class I genes, SLA-1, -2 and -3. Immunogenetics 55: 583.
23. Ando A, Ota M, Sada M, Katsuyama Y, Goto R, et al (2005) Rapid assignment of the swine major histocompatibility complex (SLA) class I and II genotypes in Clawn miniature swine using PCR-SSP and PCR-RFLP methods. Xenotransplantation 12: 121–126.
24. Fujishiro SH, Nakano K, Mizukami Y, Azami T, Arai Y, et al (2013) Generation of naive-like porcine-induced pluripotent stem cells capable of contributing to embryonic and fetal development. Stem Cells Dev 22: 473–482.
25. Raulet DH (2006). Missing self recognition and self tolerance of natural killer (NK) cells. Semin Immunol 18: 145–150.
26. Dressel R, Nolte J, Elsner L, Novota P, Guan K, et al (2010) Pluripotent stem cells are highly susceptible targets for syngeneic, allogeneic, and xenogeneic natural killer cells. FASEB J 24: 2164–2177.
27. Dressel R, Schindehütte J, Kuhlmann T, Elsner L, Novota P, et al (2008) The tumorigenicity of mouse embryonic stem cells and in vitro differentiated neuronal cells is controlled by the recipients' immune response. PLoS One 3: e2622.
28. Koch CA, Jordan CE, Platt JL (2006) Complement-dependent control of teratoma formation by embryonic stem cells. Immunol 177: 4803–4809.
29. Li Y, Lin F (2012) Mesenchymal stem cells are injured by complement after their contact with serum. Blood 120: 3436–3443.
30. Kazatchkine MD, Fearon DT, Austen KF (1979) Human alternative complement pathway: membrane-associated sialic acid regulates the competition between B and beta1 H for cell-bound C3b. J Immunol. 122: 75–81.
31. Oldenborg PA, Zheleznyak A, Fang YF, Lagenaur CF, Gresham HD, et al (2000) Role of CD47 as a marker of self on red blood cells. Science 288: 2051–2054.
32. Ide K, Wang H, Tahara H, Liu J, Wang X, et al (2007) Role for CD47-SIRP signaling in xenograft rejection by macrophages. Proc Natl Acad Sci USA 104: 5062–5066.
33. Jaiswal S, Jamieson CH, Pang WW, Park CY, Chao MP, et al (2009) CD47 is upregulated on circulating hematopoietic stem cells and leukemia cells to avoid phagocytosis. Cell 138: 271–285.
34. Kim D, Wang J, Willingham SB, Martin R, Wernig G, et al (2012) Anti-CD47 antibodies promote phagocytosis and inhibit the growth of human myeloma cells. Leukemia 26: 2538–2545.
35. Kishi Y, Tanaka Y, Shibata H, Nakamura S, Takeuchi K, et al (2008) Variation in the incidence of teratoma s after the transplantation of nonhuman primate ES cells into immunodeficient mice. Cell transplant 17: 1095–1102.
36. Hanekamp JS, Okumi M, Tena A, Arn S, Yamada K, et al (2009) Cytoplasmic inheritance of transplantation antigens in animals produced by nuclear transfer. Transplantation 88: 30–37.
37. Dhodapkar KM, Feldman D, Matthews P, Radfar S, Pickering R, et al (2010) Natural immunity to pluripotency antigen OCT4 in humans. Proc Natl Acad Sci USA 107: 8718–8723.
38. Kurre P, Pulsipher M, Woolfrey A, Maris M, Sandmaier B (2003) Reduced toxicity and prompt engraftment after minimal conditioning of a patient with Fanconi anemia undergoing hematopoietic stem cell transplantation from an HLA-matched unrelated donor. J Pediatr Hematol Oncol 25: 581–583.
39. Shook DR, Triplett BM, Srinivasan A, Hartford C, Dallas MH, et al (2013) Successful allogeneic hematopoietic cell engraftment after a minimal conditioning regimen in children with relapsed or refractory solid tumors. Biol Blood Marrow Transplant 2: 291–297.

Journal of Reproduction and Development, Vol. 60, No 3, 2014

—Original Article—

Transgenic Pigs with Pancreas-specific Expression of Green Fluorescent Protein

Hitomi MATSUNARI[1–3], Toshihiro KOBAYASHI[3,4]#, Masahito WATANABE[1,2], Kazuhiro UMEYAMA[1,2], Kazuaki NAKANO[2], Takahiro KANAI[2], Taisuke MATSUDA[2], Masaki NAGAYA[1,2], Manami HARA[5], Hiromitsu NAKAUCHI[3,4] and Hiroshi NAGASHIMA[1–3]

[1]*Meiji University International Institute for Bio-Resource Research, Kawasaki 214-8571, Japan*
[2]*Laboratory of Developmental Engineering, Department of Life Sciences, School of Agriculture, Meiji University, Kawasaki 214-8571, Japan*
[3]*Nakauchi Stem Cell and Organ Regeneration Project, ERATO, Japan Science and Technology Agency, Tokyo 102-0075, Japan*
[4]*Division of Stem Cell Therapy, Center for Stem Cell Biology and Medicine, Institute of Medical Science, The University of Tokyo, Tokyo 108-8639, Japan*
[5]*Department of Medicine, The University of Chicago, IL 60637, USA*
#*Present: Wellcome Trust /Cancer Research UK Gurdon Institute, University of Cambridge, Cambridge CB2 1QN, UK*

Abstract. The development and regeneration of the pancreas is of considerable interest because of the role of these processes in pancreatic diseases, such as diabetes. Here, we sought to develop a large animal model in which the pancreatic cell lineage could be tracked. The pancreatic and duodenal homeobox-1 (*Pdx1*) gene promoter was conjugated to Venus, a green fluorescent protein, and introduced into 370 *in vitro*-matured porcine oocytes by intracytoplasmic sperm injection-mediated gene transfer. These oocytes were transferred into four recipient gilts, all of which became pregnant. Three gilts were sacrificed at 47–65 days of gestation, and the fourth was allowed to farrow. Seven of 16 fetuses obtained were transgenic (Tg) and exhibited pancreas-specific green fluorescence. The fourth recipient gilt produced a litter of six piglets, two of which were Tg. The founder Tg offspring matured normally and produced healthy first-generation (G1) progeny. A postweaning autopsy of four 27-day-old G1 Tg piglets confirmed the pancreas-specific Venus expression. Immunostaining of the pancreatic tissue indicated the transgene was expressed in β-cells. Pancreatic islets from Tg pigs were transplanted under the renal capsules of NOD/SCID mice and expressed fluorescence up to one month after transplantation. Tg G1 pigs developed normally and had blood glucose levels within the normal range. Insulin levels before and after sexual maturity were within normal ranges, as were other blood biochemistry parameters, indicating that pancreatic function was normal. We conclude that *Pdx1-Venus* Tg pigs represent a large animal model suitable for research on pancreatic development/regeneration and diabetes.
Key words: ICSI-mediated gene transfer, Pancreas generation, Pdx1, Transgenic pig, Venus

(**J. Reprod. Dev. 60:** 230–237, 2014)

The development and utilization of genetically modified pigs have contributed to the expansion of many biomedical research efforts. For example, genetically modified pigs serving as disease models for retinitis pigmentosa [1], diabetes [2, 3], and cystic fibrosis [4, 5] have been produced, and these models are expected to further the development of new drugs and treatment methods. In xenotransplantation research, α1,3-galactosyltransferase gene knockout pigs and pigs carrying human complement regulatory factor genes have been produced (for review, see [6, 7]) and are now being used in preclinical experiments, such as the transplantation of swine organs to monkeys. Additionally, pigs expressing fluorescent proteins are exceptionally useful in research on topics such as cell tracking [8, 9] and tissue regeneration [10]. Even more innovative and more widely applicable research results are likely to be obtained through the future use of genetically modified pigs. The aim of our research was to produce transgenic (Tg) pigs to advance research on pancreas generation.

Overcoming diabetes is a global challenge for modern society; thus, the production of Tg pigs that can be used to understand the mechanisms underlying pancreatic development and the control of pancreatic functions is of great value. We therefore embarked on a program to produce Tg pigs that express the Venus variant of green fluorescent protein (GFP) [11] under the control of the pancreatic duodenal homeobox-1 (*Pdx1*) gene promoter. *Pdx1* functions as a master gene that induces the differentiation of β-cells from pancreatic stem cells, and research on Pdx1-positive cells is important for understanding the development of the pancreas and β-cell differentiation [12, 13]. The study of Pdx1-positive pancreatic stem cells may also lead to improved pathophysiological analysis and the development of treatments [13].

Methods for producing Tg pigs include pronuclear DNA injection [14], somatic cell nuclear transfer [15] and intracytoplasmic

Received: January 14, 2014
Accepted: March 11, 2014
Published online in J-STAGE: April 21, 2014

Correspondence: H Nagashima (hnagas@isc.meiji.ac.jp)

sperm injection-mediated gene transfer (ICSI-MGT) [16]. We chose ICSI-MGT for the present study, having previously confirmed that ICSI-MGT to *in vitro*-matured (IVM) porcine oocytes enables the production of Tg pigs with a high potential for reproducibility [2, 17].

In the present study, we first produced several Tg pig fetuses by ICSI-MGT to confirm that the transferred *Pdx1-Venus* gene was expressed exclusively in the pancreas. Then, we produced Tg pigs and examined their progeny to determine whether the genes were transmitted to the succeeding generation, confirming the reproducibility of the pattern of pancreas-specific expression. We further transplanted pancreatic islets of the *Pdx1-Venus* Tg pig to immunodeficient mice to verify their *in vivo* traceability. The utility of the *Pdx1-Venus* Tg pigs as a model for research on pancreatic development is discussed.

Materials and Methods

Animal care

All animal experiments in this study were approved by the Institutional Animal Care and Use Committee of Meiji University (IACUC-07-0005).

Chemicals

All chemicals were purchased from the Sigma Aldrich Chemical (St. Louis, MO, USA) unless otherwise indicated.

Construction of the Pdx1-Venus transgene

The *Pdx1-Venus* transgene construct (8.4 kb) consisted of the mouse *Pdx1* promoter, *Venus* cDNA, and rabbit β-globin gene sequence (from partway through the second exon to the 3' untranslated region), including a polyadenylation signal (pA) (Fig. 1). The transgene fragment was excised from the plasmid vector by enzymatic digestion using the *Bss*HII restriction enzyme (Takara Bio, Shiga, Japan), separated by gel electrophoresis, and purified using the QIAquick® Gel Extraction Kit (QIAGEN, Hilden, Germany).

In vitro maturation of oocytes

Porcine ovaries were collected at a local abattoir and transported to the laboratory in Dulbecco's phosphate buffered saline (DPBS, Nissui Pharmaceutical, Tokyo, Japan) containing 75 μg/ml potassium penicillin G, 50 μg/ml streptomycin sulfate, 2.5 μg/ml amphotericin B, and 0.1% (w/v) polyvinyl alcohol (PVA). Cumulus-oocyte complexes were collected from the ovarian antral follicles (3.0 to 6.0 mm in diameter) by aspiration with a 10-ml syringe and a 20 G hypodermic needle, and those with at least three layers of compacted cumulus cells were selected and cultured in NCSU23 medium [18] supplemented with 0.6 mM cysteine, 10 ng/ml epidermal growth factor, 10% (v/v) porcine follicular fluid, 75 μg/ml potassium penicillin G, 50 μg/ml streptomycin sulfate, 10 IU/ml eCG (ASKA Pharmaceutica, Tokyo, Japan), and 10 IU/ml hCG (ASKA Pharmaceutical) at 38.5 C in a humidified atmosphere of 5% CO_2 in air for 22 h. Then, the oocytes were cultured for an additional 21 h without eCG and hCG at 38.5 C in a humidified atmosphere of 5% CO_2, 5% O_2, and 90% N_2 [19]. IVM oocytes with expanded cumulus cells were treated with 1 mg/ml hyaluronidase dissolved in Tyrode lactose medium containing 10 mM HEPES and 0.3% (w/v) polyvinylpyrrolidone (TL-HEPES-PVP) and separated from the cumulus cells by gentle pipetting. Oocytes with an evenly granulated ooplasm and an extruded first polar body were selected for the subsequent experiments.

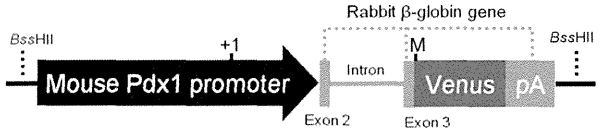

Fig. 1. Structure of an expression vector for the *Pdx1-Venus* cDNA. A schematic presentation of the *Pdx1-Venus* transgene used to generate transgenic pigs. The fusion gene (8.4 kb) consists of 6.5 kb of the mouse Pdx1 promoter and a rabbit β-globin gene including an insertion of 0.72 kb Venus cDNA in the 3rd exon and a polyadenylation signal in the 3' –flanking region. Transcription and translation start site are indicated by +1 and M, respectively.

Porcine sperm preparation for ICSI-MGT

Commercially available boar semen (Duroc) suitable for artificial insemination was used to prepare frozen sperm for ICSI-MGT. Beltsville thawing solution (BTS) was used as a freezing solution without cryoprotective agents [20]. The sperm were washed three times by centrifugation at 200 × *g* for 5 min in BTS to remove the extender. The sperm were then suspended in BTS (containing 5% (w/v) BSA) at a concentration of 3×10^7 cells/ml, placed in 0.25-ml plastic freezing straws (Fujihira Industry, Tokyo, Japan), and plunged into liquid nitrogen. The straws of frozen sperm were thawed by soaking in a 37 C water bath for 10 sec. The sperm recovered from the straws were washed twice in BTS (containing 0.1% (w/v) BSA), suspended in Nucleus Isolation Medium (NIM) [21], and used in ICSI-MGT within 60 min of thawing. For tail removal by sonication, an ultrasonic sonicator (Honda Electronics, Aichi, Japan) was used to apply ultrasonic vibrations (100 W, 28 kHz) for 9 sec to 300 μl of the sperm suspension (5×10^7 cells/ml) in a 1.5-ml microcentrifuge tube. This duration of sonication was determined to decapitate approximately 70% of the sperm. Sperm that had been subjected to tail removal by sonication were resuspended in NIM at a concentration of $2–5 \times 10^4$ cells/μl. Next, the DNA solution was added to the sperm suspension to yield a concentration of 2.5 ng/μl. The suspension was then gently mixed and incubated at room temperature for 5 min. The resulting sperm were stored on ice until use in ICSI-MGT.

Intracytoplasmic sperm injection

The IVM oocytes at 43–45 h after commencement of the maturation culture were activated by electrical stimulation before the injection of sperm heads. The oocytes were lined up between two wire electrodes (1.0 mm apart) of a fusion chamber (CUY500G1, Nepa Gene, Chiba, Japan) and overlaid with an activation solution, consisting of 0.28 M mannitol (Nacalai Tesque, Kyoto, Japan), 50 μM $CaCl_2$, 100 μM $MgSO_4$, and 0.01% (w/v) PVA. Activation was induced with one DC pulse of 150 V/mm for 100 μsec using an electric pulsing machine (ET-1, Fujihira Industry).

ICSI-MGT was performed in a 4-μl drop of TL-HEPES-PVP under mineral oil using an Nikon inverted microscope (TE-300,

Nikon, Tokyo, Japan) as described previously [17]. Approximately 1 μl of sperm suspension that had been co-incubated with DNA was transferred to a 2-μl drop of 10% (w/v) PVP (in DPBS; Irvine Scientific, Sales, Santa Ana, CA, USA). Sperm heads were aspirated from the PVP drop using an injection pipette and moved to the drop containing the oocytes. An oocyte was first captured by a holding pipette. Next, with the oocyte immobilized with its polar body at either the 6- or 12-o'clock position, a sperm head was injected using the piezo-actuated microinjection unit (PMM-150FU, Prime Tech, Tsuchiura, Japan) and micromanipulators (MO-202U, Narishige, Tokyo, Japan). Sperm injection was carried out within 30 min of activation of the oocytes.

After ICSI-MGT, embryos to be transferred to recipients were cultured in Porcine Zygote Medium-5 (PZM-5, Research Institute for the Functional Peptides, Yamagata, Japan) for 1–3 days under a humidified atmosphere of 5% CO_2, 5% O_2, and 90% N_2 at 38.5 C.

Embryo transfer

Crossbred (Large White/Landrace × Duroc) prepubertal gilts weighing from 100 to 105 kg were used as recipients of the sperm-injected embryos. The gilts were treated with a single intramuscular injection of 1000 IU of eCG to induce estrus. Ovulation was induced by an intramuscular injection of 1500 IU of hCG (Kawasaki Pharmaceutical, Kanagawa, Japan) given 66 h after the injection of eCG. Sperm-injected embryos cultured for 1–3 days were surgically transferred into the oviducts of recipients approximately 48 h or 72 h after hCG injection.

All but one of the pregnant recipients were laparotomized to recover fetuses at 47–65 days of gestation, and the remaining recipient was allowed to farrow.

PCR and Southern blot analyses

Genomic DNA was extracted from tail biopsies of fetuses and newborn piglets using proteinase K (Life Technologies Corporation, Carlsbad, CA, USA) and purified by the phenol-chloroform method. To identify Tg pigs, DNA samples were analyzed by PCR using the following primers: 5'-caatgatggctccagggtaa (forward) and 5'-ctccttgaagtcgatgccctt (reverse).

For Southern blot analysis, genomic DNA extracted as described above was digested with the *Pst*I restriction enzyme (Takara Bio), separated by gel electrophoresis, and transferred onto a nylon membrane (GE Healthcare, Buckinghamshire, UK), which was then hybridized with the DIG-labeled probes prepared by PCR using the following primers: 5'-caatgatggctccagggtaa (forward) and 5'-ggtggtgcagatcagcttca (reverse). The signal (i.e., binding of the probe) was detected by chromogenic methods. The number of transgene copies integrated into the porcine genome was determined by comparison of the hybridization signal with that of the copy-number control, which was diluted to make a standard series (1–100 copies per diploid genome).

Pancreas-specific fluorescence expression in Tg fetuses and G1 offspring

The tails of the fetuses (day 47–65) obtained from autopsies of the sacrificed pregnant pigs were used to extract genomic DNA. Tg fetuses were identified by PCR. Fetal viscera were also removed, and the expression of green fluorescence in the organs was analyzed by fluorescence stereomicroscopy (MVX10, Olympus, Tokyo, Japan; excitation wavelength of 460–480 nm; absorption filter of 495–540 nm). Pancreatic tissue samples from fetuses were fixed in 4% paraformaldehyde and used to prepare paraffin-embedded sections (hematoxylin/eosin stain). The paraffin-embedded sections were also analyzed by fluorescence microscopy (Olympus BX52; excitation wavelength of 460–480 nm; absorption filter of 495–540 nm).

A subset of the founder Tg pigs was allowed to grow to maturity and was mated with wild-type pigs. The offspring (G1) obtained were sacrificed when they reached the age of 27 days to examine pancreas-specific fluorescence expression by fluorescence stereomicroscopy.

Pancreatic tissue samples of the founder Tg pig (G0) were double-stained using anti-insulin (1:500; LS-C24686, LifeSpan BioSciences, Seattle, WA, USA) and anti-GFP (1:500-1:1000; #598, MBL, Nagoya, Japan) antibodies to determine the Venus-expressing cells in the pancreatic islets. Alexa Fluor® 594 goat anti-guinea pig IgG (A11076, Life Technologies) and Alexa Fluor® 488 donkey anti-rabbit IgG (A21206, Life Technologies) were used as the secondary antibodies. The tissue sections were also double-stained for glucagon and Venus. For glucagon staining, anti-glucagon antibody (1:500; G2654) and Alexa Fluor®594 goat anti-mouse IgG (A11020, Life Technologies) were employed. After antibody treatments, the sections were mounted in Vectashield mounting medium (Vector Laboratories, Burlingame, CA, USA) containing 4′,6-diamidino-2-phenylindole (DAPI) for nuclear counterstaining and observed by confocal laser scanning microscopy (FV1000-D; Olympus, Tokyo, Japan).

Fluorescence in situ hybridization (FISH)

Peripheral blood cells derived from the two Tg founder pigs (male and female) were cultured in RPMI1640 containing 20% (v/v) FBS for 3 days. The cells were then cultured with 30 μg/ml BrdU for 5 h, followed by incubation with 0.02 μg/ml colcemide for 1 h. After fixation with methanol-acetic acid (3:1 ratio), the cells were spread on slides and air-dried. The cells were then stained with Hoechst 33258 and treated with UV light for G-banding. *Pdx1-Venus* DNA was labeled with Cy3 as a probe and hybridized at 37 C overnight. After stringent washing, the bound label was detected with anti–Dig-Cy3 using Leica DRAM2 and CW4000 FISH software.

Tracing of pancreatic islets by fluorescence after ectopic transplantation

Pancreatic islets were isolated from a 4.5-month-old Tg pig using a conventional method. The pancreas collected from a Tg pig was distended by infusion with Liberase DL (Roche Diagnostics, Indianapolis, IN, USA) suspended in Hank's balanced salt solution (HBSS; Life Technologies), followed by a static incubation in an empty 125 ml storage bottle for 30 min at 37 C. Then the digesting pancreatic tissue was gently shaken with 7 mm Teflon® beads in RPMI 1640 (Life Technologies). Digestion was terminated by the addition of cold HBSS containing 10% (v/v) FBS, 100 IU/ml of penicillin, 100 mg/ml of streptomycin, and 2.5 μg/ml amphotericin B. The digested tissue was passed through a 500 μm stainless steel mesh screen. The tissue effluent was collected in 50 ml conical tubes and centrifuged for 2 min at 155 × *g* at 4 C. The islets were purified using a Histopaque®-1.077 gradient with RPMI 1640. Following

Table 1. Efficiency of the ICSI-MGT method for the production of Tg pig fetuses and offspring carrying the *Pdx1-Venus* gene

	Recipient	No. of embryos transferred	Production efficiency of fetuses or offspring (%)*1	Production efficiency of Tg fetuses or offspring (%)*2
Fetus	W8	83	8.4 [7/83]	28.6 [2/7]
	W9	81	3.7 [3/81]	100 [3/3]
	W11	79	7.6 [6/79]	33.3 [2/6]
Offspring	W10	127	4.7 [6/127]	33.3 [2/6]

*1 No. of fetuses or piglets / No. of embryos transferred × 100. *2 No. of Tg fetuses or piglets / No. of fetuses or piglets obtained × 100.

Table 2. Expression of the *Pdx1-Venus* gene in Tg pig fetuses produced by the ICSI-MGT method

Fetus	Fetal age	Fetal sex	Fluorescence intensity	Transgene copy number
W8-1	Day 48	F	+	30
W8-5	Day 48	F	+	5
W9-1	Day 47	F	+	5
W9-2	Day 47	M	++	15
W9-3	Day 47	M	++	70
W11-2	Day 65	F	+	5
W11-5	Day 65	F	++	100≤

centrifugation at 1700 × *g* for 17 min at 4 C, the islets were collected from the interface between the RPMI 1640 and Histopaque®-1.077. Purified islets were washed by centrifugation at 155 × *g* for 2 min at 4 C in RPMI 1640 supplemented with 10% (v/v) FBS. The purity of the isolated islets was confirmed to be over 90% by microscopic inspection after Dithizone (5 mg/ml, in DPBS) staining.

Fluorescence in the isolated islets was observed by fluorescence stereoscopic microscopy (MVX10, Olympus). Isolated islets were then transplanted under the renal capsules of anesthetized NOD/SCID mice (CLEA Japan, Tokyo, Japan). Kidneys were removed either immediately or at one month after transplantation and analyzed by fluorescence stereomicroscopy (MVX10, Olympus) to determine whether the islets could be traced using Venus fluorescence as an indicator.

Results

Efficiency of production of Pdx1-Venus Tg pigs by ICSI-MGT

The ICSI-MGT method was selected for creating *Pdx1-Venus* Tg pigs. In total, 370 sperm-injected embryos were transferred into four recipients, all of which became pregnant.

Three of the recipient pigs were autopsied at 47–65 days of gestation, and 16 fetuses were recovered for analysis (Table 1). The production efficiency of fetuses was between 4 and 8%, as each recipient received approximately 80 embryos. Seven of the 16 fetuses were Tg (43.8%), including approximately 30% of the fetuses in two of the recipients and all three fetuses in one recipient. Overall, 2.4–3.7% of the transferred embryos produced Tg fetuses.

The fourth pregnant pig, which received 127 embryos, was allowed to farrow and produced six (4.7%) piglets, two of which were Tg (one female and one male).

Pancreas-specific expression of Venus in Tg fetuses and offspring

The viscera of the seven Tg fetuses obtained were examined by fluorescence stereomicroscopy, and we found that all the fetuses had pancreas-specific expression of Venus fluorescence (Fig. 2A and B). The Southern blot analysis of genomic DNAs indicated an integration of 5 to 100 copies of the gene. Although the fluorescence intensity tended to be greater in fetuses with higher copy numbers (≥15), except for a female fetus (W8-1) harboring 30 copies of the gene, pancreas-specific expression was clear in all fetuses regardless of the copy number (Table 2).

A histological analysis of pancreatic tissues of four Tg fetuses showed that Venus fluorescence was present in cells determined to be acinar cells based on their appearance. This expression pattern was consistent among all fetuses analyzed (Fig. 2C and D).

The two founder (G0; male and female) Tg pigs grew normally to adulthood and were crossed with wild-type pigs to produce G1 offspring of six litters. Of the 22 G1 pigs obtained from the male founder and the 28 G1 pigs derived from the female founder, the transgene was transmitted to 10 (45.5%) and 16 pigs (57.1%), respectively, indicating that the transgene was transmitted in the Mendelian fashion. It was found that 10 and 30 transgene copies were integrated into the genomes of the male and female founder pigs, respectively. FISH analysis of these founder Tg pigs revealed that concatemerized transgenes were integrated into a single site on the chromosomes (Suppl. Fig. 1: on-line only).

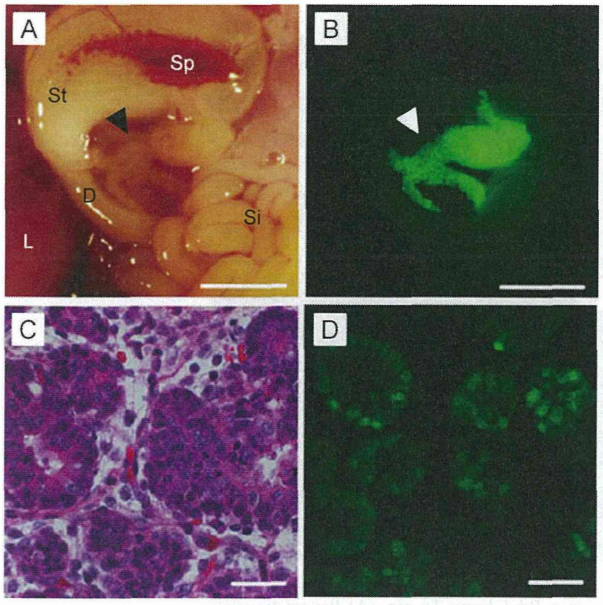

Fig. 2. Pancreas-specific expression of the *Pdx1-Venus* gene in the Tg pig fetus. Bright-field (A) and fluorescence microscopic (B) observation of the pancreas (arrowheads). Acinar cells (C, HE stain) showed prominent Venus expression (D). D, duodenum; L, liver; Si, small intestine; Sp, spleen; St, stomach. Scale bars = 5 mm (A, B); 50 μm (C, D).

Four 27-day-old G1 piglets (Tg female and male, non-Tg female and male) were autopsied to examine fluorescence expression in their viscera. The pancreas, duodenum, small intestine, liver, spleen, kidneys, skin, heart, lungs, and stomach were observed under a fluorescence stereomicroscope. This analysis confirmed the retention of pancreas-specific fluorescence expression (Fig. 3A and Suppl. Fig. 2: on-line only) as in the founder Tg fetuses. Green fluorescence was not detected in the viscera of non-Tg pigs.

The pancreatic tissue of the G1 Tg pigs showed green fluorescent spots throughout (Fig. 3A), indicating *Pdx1-Venus* expression in islets. Venus expression was found to be confined to β-cells in the pancreatic tissue after double staining with anti-insulin and anti-GFP antibodies (Fig. 3B).

Tracing of the fluorescence expression of pancreatic islets

To further examine the potential of *Pdx1-Venus* Tg pigs for future use in pancreatic islet research, we investigated the traceability of the pancreatic islets using their fluorescence as an indicator. As shown in Fig. 4, Venus fluorescence expression patterns were clearly observed under a fluorescence stereomicroscope, which confirmed clear fluorescence spots in the islets (Fig. 4A and A').

The isolated islets were transplanted under the renal capsules of NOD/SCID mice, and the transplanted islets could clearly be identified by their fluorescence. The fluorescence of the transplanted pancreatic islets was still clear at 30 days after transplantation (Fig. 4C and C').

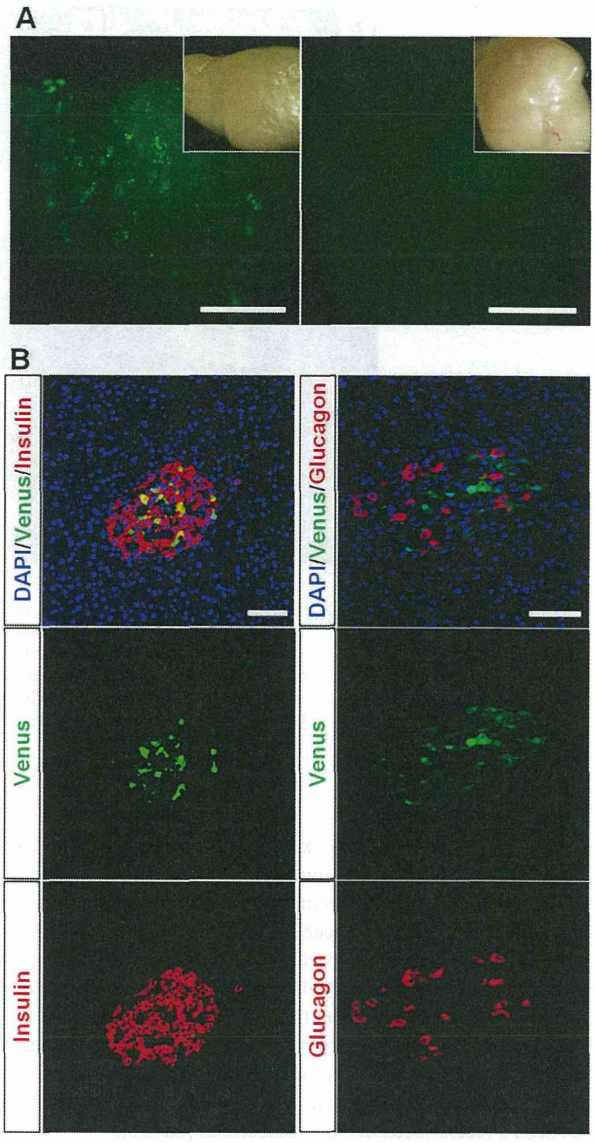

Fig. 3. Expression of the *Pdx1-Venus* gene in the pancreas of a Tg pig. (A) Green fluorescent spots were observed by fluorescence stereomicroscopy throughout the pancreatic tissue of the Tg pigs (left panel), indicating *Pdx1-Venus* expression in islets. Right panel: pancreatic tissue of a control wild-type pig. The inset in each panel presents a bright-field image of the tissue. Scale bars = 2.5 mm. (B) Immunohistochemical staining of pancreatic islets of a *Pdx1-Venus* Tg pig. Merged images of the Tg pig islet demonstrated that the expression of the *Pdx1-Venus* gene was confined to β-cells (top left), whereas this gene was not expressed in glucagon-producing cells (top right). Scale bars = 50 μm.

Discussion

This report describes the production of the first *Pdx1-Venus* Tg pig expressing green fluorescent protein specifically in the pancreas,

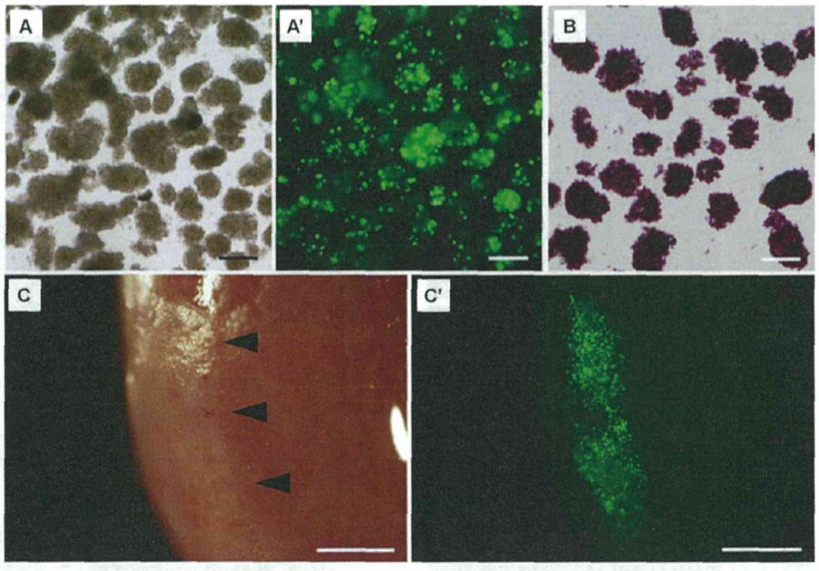

Fig. 4. Fluorescence of pancreatic islets isolated from a *Pdx1-Venus* Tg pig. (A) Pancreatic islets isolated from a Tg pig. (A') Fluorescent spots were observed in the islets of a Tg pig. (B) Dithizone-stained islets of a Tg pig. (C, C') Pancreatic islets of a *Pdx1-Venus* Tg pig transplanted into the kidney capsule of NOD/SCID mice (arrowheads). Bright-field (C) and fluorescence (C') observation by fluorescence stereomicroscopy showed that the fluorescence of the transplanted islets was clear at 30 days after transplantation (A'). Scale bars = 200 μm (A–C); 1 mm (C, C').

particularly in β-cells. Pdx1 is a key molecule with an important role in pancreatic stem cell differentiation into β-cells [12, 13, 22, 23]. In fact, *Pdx1* knockout mice reportedly suffer impaired pancreatic development [12, 24]. The identification and separation of *Pdx1*-positive cells is therefore expected to stimulate new developments in research on islet architecture during the ontogeny and differentiation of β-cells from precursors [13, 25, 26]. Research on pancreas development and β-cell differentiation is also expected to lead to the pathophysiological analysis of diabetes and the development of new therapeutic methods [27]. In particular, the neogenesis of β-cells has been a recent focus in diabetes research [28–31].

In research using laboratory rodents, $Pdx1^{GFP/w}$ mice [32] and mouse insulin I gene promoter (MIP)-GFP Tg mice [33] have been created and used to conduct research on pancreatic development and differentiation. However, in research using pigs, a Tg model that is useful for the study of β-cell biology, including the identification of progenitor cells, has not been available. Considering that the importance of pigs, as a large laboratory animal with several similarities to humans, in translational research is now recognized and that research is being undertaken on the clinical applications of porcine islet transplantation [34], the *Pdx1-Venus* pig we have produced has strong potential for use as an effective research tool. The Expression pattern of the *Pdx1-Venus* in the islet of our transgenic pigs was similar to that reported previously in the $Pdx1^{GFP/w}$ mice [32].

In the present study, we employed the mouse *Pdx1* promoter to drive the *Venus* expression in the transgenic pigs. However the transgene was expressed in a highly tissue-specific manner. In fact, *Pdx1-Venus* expression was confined to the pancreas during the early fetal stage (day 47) and at the adult stage. *Pdx1* is also known to be expressed in the duodenum at the fetal stage [13]. Further studies need to be undertaken to examine the expression of the *Pdx1-Venus* in the early stages of pancreatogenesis in the transgenic pig fetuses.

Concerning *Pdx1-Venus* expression in the islets, we observed that cells that were Venus positive were also insulin-positive cells. This pig is, accordingly, very useful for tracking the behavior of pancreatic progenitor cells and β-cells.

Pdx1-Venus is also useful as a cell marker following islet transplantation. The clinical application of islet transplantation using human islets has been hampered, as is the case with other transplants, by the shortage of donor organs. However, if xenogeneic pancreas transplantation—more specifically, the transplantation of pig islets to humans—becomes possible, substantial advances will be made in treatments for diabetes patients [35]. Xenogeneic transplantation will require further basic studies, including a long-term follow-up of islets transplanted to animals. *Pdx1-Venus* Tg pig islets will serve as a very useful tool in such research. For example, production of insulin or C-peptide from the transplanted islets may be correlated with the *Pdx1-Venus* expression that indicates the viability of β-cells. We have already produced diabetic model Tg pigs by mutant hepatocyte nuclear factor-1α gene transfer [2]. Transplanting islets from *Pdx1-Venus* Tg pigs using such diabetic models should provide knowledge that can be extrapolated from large animals to humans.

Pdx1-Venus Tg pigs were observed to show a high level of green fluorescence expression in the pancreas (β-cells) with normal pancreas

function. This finding was confirmed by the pigs' physiological characteristics, including growth, casual blood glucose levels, postprandial blood glucose and insulin levels, and blood biochemical parameters, which were measured during the period from the postweaning through the growth stages (Suppl. Text, Suppl. Fig. 3, and Suppl. Table 1: on-line only). Based on these results, we hypothesize that *Pdx1-Venus* Tg pigs may also be suitable as donor animals in studies of islet transplantation.

In this study, we introduced transgenes using the ICSI-MGT method. We previously reported that the application of ICSI-MGT is highly effective for introducing exogenous genes to porcine IVM oocytes [2, 17]. In this study, approximately 30–100% of the fetuses/piglets obtained in each litter were Tg, once more demonstrating the high efficiency of the ICSI-MGT method. The production efficiency of Tg fetuses or piglets obtained in this study was equal or rather higher compared with our previous studies, probably due to lower detrimental effect of the transgene expression [2, 36, 37]. *In vitro* maturation of pig oocytes is now an established method, and the combination of IVM oocytes and the ICSI-MGT method can accordingly be considered a practical method for generating Tg pigs.

Our previous research confirmed that transgenes introduced by the ICSI-MGT method generally insert into a single site on the host genome as concatemers [17, 38]. In the founder Tg pigs used for generating G1 offspring in this study, it was shown that the transgenes did concatamerize and integrated into a single site of the chromosome as shown in our previous studies [17, 38]. No significant differences in growth were observed in fetuses with transgene copy numbers between 5 and 100. The level of transgene expression is considered to be more readily influenced by the integration site on the chromosome than by the integrated copy number [39, 40]. Even so, in the case of Tg individuals with an exceptionally high number of integrated transgenes, it is possible that high-level transgene expression may influence normality in piglets and affect their long-term survival. Because the copy number of the integrated genes is affected by various factors related to the binding of DNA to sperm [38, 41, 42], the preliminary optimization of the transgene-sperm co-incubation will be critical for the efficient production of Tg pigs using the ICSI-MGT method.

In conclusion, building on our current knowledge, this study verifies that using IVM oocytes and ICSI-MGT together is an effective method for producing Tg pigs. Additionally, because the *Pdx1-Venus* Tg pigs produced in this study express green fluorescent protein specifically in the pancreas (β-cells) and maintain normal physiological function, we can conclude that this large animal model is suitable for research on pancreatic development and regeneration as well as diabetes.

Acknowledgments

This work was supported by the Japan Science and Technology Agency, ERATO, Nakauchi Stem Cell and Organ Regeneration Project, JSPS KAKENHI Grant Number 24659596, and the Meiji University International Institute for Bio-Resource Research (MUIIBR).

References

1. **Petters RM, Alexander CA, Wells KD, Collins EB, Sommer JR, Blanton MR, Rojas G, Hao Y, Flowers WL, Banin E, Cideciyan AV, Jacobson SG, Wong F.** Genetically engineered large animal model for studying cone photoreceptor survival and degeneration in retinitis pigmentosa. *Nat Biotechnol* 1997; **15**: 965–970. [Medline] [CrossRef]
2. **Umeyama K, Watanabe M, Saito H, Kurome M, Tohi S, Matsunari H, Miki K, Nagashima H.** Dominant-negative mutant hepatocyte nuclear factor 1alpha induces diabetes in transgenic-cloned pigs. *Transgenic Res* 2009; **18**: 697–706. [Medline] [CrossRef]
3. **Renner S, Fehlings C, Herbach N, Hofmann A, von Waldthausen DC, Kessler B, Ulrichs K, Chodnevskaja I, Moskalenko V, Amselgruber W, Göke B, Pfeifer A, Wanke R, Wolf E.** Glucose intolerance and reduced proliferation of pancreatic beta-cells in transgenic pigs with impaired glucose-dependent insulinotropic polypeptide function. *Diabetes* 2010; **59**: 1228–1238. [Medline] [CrossRef]
4. **Rogers CS, Stoltz DA, Meyerholz DK, Ostedgaard LS, Rokhlina T, Taft PJ, Rogan MP, Pezzulo AA, Karp PH, Itani OA, Kabel AC, Wohlford-Lenane CL, Davis GJ, Hanfland RA, Smith TL, Samuel M, Wax D, Murphy CN, Rieke A, Whitworth K, Uc A, Starner TD, Brogden KA, Shilyansky J, McCray PB Jr, Zabner J, Prather RS, Welsh MJ.** Disruption of the CFTR gene produces a model of cystic fibrosis in newborn pigs. *Science* 2008; **321**: 1837–1841. [Medline] [CrossRef]
5. **Klymiuk N, Mundhenk L, Kraehe K, Wuensch A, Plog S, Emrich D, Langenmayer MC, Stehr M, Holzinger A, Kröner C, Richter A, Kessler B, Kurome M, Eddicks M, Nagashima H, Heinritzi K, Gruber AD, Wolf E.** Sequential targeting of *CFTR* by BAC vectors generates a novel pig model of cystic fibrosis. *J Mol Med (Berl)* 2012; **90**: 597–608. [Medline] [CrossRef]
6. **Miyagawa S, Yamamoto A, Matsunami K, Wang D, Takama Y, Ueno T, Okabe M, Nagashima H, Fukuzawa M.** Complement regulation in the GalT KO era. *Xenotransplantation* 2010; **17**: 11–25. [Medline] [CrossRef]
7. **Matsunari H, Watanabe M, Umeyama K, Nakano K, Kurome M, Kessler B, Wolf E, Miyagawa S, Nagashima H.** Cloning of homozygous α1,3-galactosyltransferase gene knock-out pigs by somatic cell nuclear transfer. In: Miyagawa S (ed.), Xenotransplantation. Rijeka, Croatia: InTech; 2012: 37-54.
8. **Lai L, Park KW, Cheong HT, Kühholzer B, Samuel M, Bonk A, Im GS, Rieke A, Day BN, Murphy CN, Carter DB, Prather RS.** Transgenic pig expressing the enhanced green fluorescent protein produced by nuclear transfer using colchicine-treated fibroblasts as donor cells. *Mol Reprod Dev* 2002; **62**: 300–306. [Medline] [CrossRef]
9. **Matsunari H, Onodera M, Tada N, Mochizuki H, Karasawa S, Haruyama E, Nakayama N, Saito H, Ueno S, Kurome M, Miyawaki A, Nagashima H.** Transgenic-cloned pigs systemically expressing red fluorescent protein, Kusabira-Orange. *Cloning Stem Cells* 2008; **10**: 313–323. [Medline] [CrossRef]
10. **Shigeta T, Hsu HC, Enosawa S, Matsuno N, Kasahara M, Matsunari H, Umeyama K, Watanabe M, Nagashima H.** Transgenic pig expressing the red fluorescent protein kusabira-orange as a novel tool for preclinical studies on hepatocyte transplantation. *Transplant Proc* 2013; **45**: 1808–1810. [Medline] [CrossRef]
11. **Nagai T, Ibata K, Park ES, Kubota M, Mikoshiba K, Miyawaki A.** A variant of yellow fluorescent protein with fast and efficient maturation for cell-biological applications. *Nat Biotechnol* 2002; **20**: 87–90. [Medline] [CrossRef]
12. **Jonsson J, Carlsson L, Edlund T, Edlund H.** Insulin-promoter-factor 1 is required for pancreas development in mice. *Nature* 1994; **371**: 606–609. [Medline] [CrossRef]
13. **Bonal C, Herrera PL.** Genes controlling pancreas ontogeny. *Int J Dev Biol* 2008; **52**: 823–835. [Medline] [CrossRef]
14. **Hammer RE, Pursel VG, Rexroad CEJ Jr, Wall RJ, Bolt DJ, Ebert KM, Palmiter RD, Brinster RL.** Production of transgenic rabbits, sheep and pigs by microinjection. *Nature* 1985; **315**: 680–683. [Medline] [CrossRef]
15. **Park KW, Cheong HT, Lai L, Im GS, Kühholzer B, Bonk A, Samuel M, Rieke A, Day BN, Murphy CN, Carter DB, Prather RS.** Production of nuclear transfer-derived swine that express the enhanced green fluorescent protein. *Anim Biotechnol* 2001; **12**: 173–181. [Medline] [CrossRef]
16. **Yong HY, Hao Y, Lai L, Li R, Murphy CN, Rieke A, Wax D, Samuel M, Prather RS.** Production of a transgenic piglet by a sperm injection technique in which no chemical or physical treatments were used for oocytes or sperm. *Mol Reprod Dev* 2006; **73**: 595–599. [Medline] [CrossRef]
17. **Kurome M, Ueda H, Tomii R, Naruse K, Nagashima H.** Production of transgenic-clone pigs by the combination of ICSI-mediated gene transfer with somatic cell nuclear transfer. *Transgenic Res* 2006; **15**: 229–240. [Medline] [CrossRef]
18. **Petters RM, Wells KD.** Culture of pig embryos. *J Reprod Fertil Suppl* 1993; **48**: 61–73. [Medline]
19. **Funahashi H, Day BN.** Effects of the duration of exposure to hormone supplements on cytoplasmic maturation of pig oocytes in vitro. *J Reprod Fertil* 1993; **98**: 179–185. [Medline] [CrossRef]
20. **Pursel VG, Johnson LA.** Freezing of boar spermatozoa: fertilizing capacity with concen-

trated semen and a new thawing procedure. *J Anim Sci* 1975; **40**: 99–102. [Medline]

21. **Kuretake S, Kimura Y, Hoshi K, Yanagimachi R.** Fertilization and development of mouse oocytes injected with isolated sperm heads. *Biol Reprod* 1996; **55**: 789–795. [Medline] [CrossRef]
22. **Wang H, Maechler P, Ritz-Laser B, Hagenfeldt KA, Ishihara H, Philippe J, Wollheim CB.** Pdx1 level defines pancreatic gene expression pattern and cell lineage differentiation. *J Biol Chem* 2001; **276**: 25279–25286. [Medline] [CrossRef]
23. **Lottmann H, Vanselow J, Hessabi B, Walther R.** The Tet-On system in transgenic mice: inhibition of the mouse pdx-1 gene activity by antisense RNA expression in pancreatic beta-cells. *J Mol Med (Berl)* 2001; **79**: 321–328. [Medline] [CrossRef]
24. **Ahlgren U, Jonsson J, Edlund H.** The morphogenesis of the pancreatic mesenchyme is uncoupled from that of the pancreatic epithelium in IPF1/PDX1-deficient mice. *Development* 1996; **122**: 1409–1416. [Medline]
25. **Holland AM, Hale MA, Kagami H, Hammer RE, MacDonald RJ.** Experimental control of pancreatic development and maintenance. *Proc Natl Acad Sci USA* 2002; **99**: 12236–12241. [Medline] [CrossRef]
26. **Herrera PL.** Adult insulin- and glucagon-producing cells differentiate from two independent cell lineages. *Development* 2000; **127**: 2317–2322. [Medline]
27. **Kilimnik G, Kim A, Steiner DF, Friedman TC, Hara M.** Intraislet production of GLP-1 by activation of prohormone convertase 1/3 in pancreatic α-cells in mouse models of ß-cell regeneration. *Islets* 2010; **2**: 149–155. [Medline] [CrossRef]
28. **Thorel F, Népote V, Avril I, Kohno K, Desgraz R, Chera S, Herrera PL.** Conversion of adult pancreatic alpha-cells to beta-cells after extreme beta-cell loss. *Nature* 2010; **464**: 1149–1154. [Medline] [CrossRef]
29. **Chung C-H, Levine F.** Adult pancreatic alpha-cells: a new source of cells for beta-cell regeneration. *Rev Diabet Stud* 2010; **7**: 124–131. [Medline] [CrossRef]
30. **Gianani R.** Beta cell regeneration in human pancreas. *Semin Immunopathol* 2011; **33**: 23–27. [Medline] [CrossRef]
31. **Wang Y, Lanzoni G, Carpino G, Cui CB, Dominguez-Bendala J, Wauthier E, Cardinale V, Oikawa T, Pileggi A, Gerber D, Furth ME, Alvaro D, Gaudio E, Inverardi L, Reid LM.** Biliary tree stem cells, precursors to pancreatic committed progenitors: evidence for possible life-long pancreatic organogenesis. *Stem Cells* 2013; **31**: 1966–1979. [Medline] [CrossRef]
32. **Holland AM, Micallef SJ, Li X, Elefanty AG, Stanley EG.** A mouse carrying the green fluorescent protein gene targeted to the Pdx1 locus facilitates the study of pancreas development and function. *Genesis* 2006; **44**: 304–307. [Medline] [CrossRef]
33. **Hara M, Wang X, Kawamura T, Bindokas VP, Dizon RF, Alcoser SY, Magnuson MA, Bell GI.** Transgenic mice with green fluorescent protein-labeled pancreatic beta -cells. *Am J Physiol Endocrinol Metab* 2003; **284**: E177–E183. [Medline]
34. **Elliott RB, Escobar L, Tan PLJ, Muzina M, Zwain S, Buchanan C.** Live encapsulated porcine islets from a type 1 diabetic patient 9.5 yr after xenotransplantation. *Xenotransplantation* 2007; **14**: 157–161. [Medline] [CrossRef]
35. **Orive G, Hernández RM, Gascón AR, Igartua M, Pedraz JL.** Encapsulated cell technology: from research to market. *Trends Biotechnol* 2002; **20**: 382–387. [Medline] [CrossRef]
36. **Watanabe M, Kurome M, Matsunari H, Nakano K, Umeyema K, Shiota A, Nakauchi H, Nagashima H.** The creation of transgenic pigs expressing human proteins using BAC-derived, full-length genes and intracytoplasmic sperm injection-mediated gene transfer. *Transgenic Res* 2012; **21**: 605–618. [Medline] [CrossRef]
37. **Matsunari H, Nagashima H, Watanabe M, Umeyama K, Nakano K, Nagaya M, Kobayashi T, Yamaguchi T, Sumazaki R, Herzenberg LA, Nakauchi H.** Blastocyst complementation generates exogenic pancreas in vivo in apancreatic cloned pigs. *Proc Natl Acad Sci USA* 2013; **110**: 4557–4562. [Medline] [CrossRef]
38. **Umeyama K, Saito H, Kurome M, Matsunari H, Watanabe M, Nakauchi H, Nagashima H.** Characterization of the ICSI-mediated gene transfer method in the production of transgenic pigs. *Mol Reprod Dev* 2012; **79**: 218–228. [Medline] [CrossRef]
39. **Clark AJ, Bissinger P, Bullock DW, Damak S, Wallace R, Whitelaw CBA, Yull F.** Chromosomal position effects and the modulation of transgene expression. *Reprod Fertil Dev* 1994; **6**: 589–598. [Medline] [CrossRef]
40. **Kong Q, Wu M, Huan Y, Zhang L, Liu H, Bou G, Luo Y, Mu Y, Liu Z.** Transgene expression is associated with copy number and cytomegalovirus promoter methylation in transgenic pigs. *PLoS ONE* 2009; **4**: e6679. [Medline] [CrossRef]
41. **Hirabayashi M, Kato M, Ishikawa A, Kaneko R, Yagi T, Hochi S.** Factors affecting production of transgenic rats by ICSI-mediated DNA transfer: effects of sonication and freeze-thawing of spermatozoa, rat strains for sperm and oocyte donors, and different constructs of exogenous DNA. *Mol Reprod Dev* 2005; **70**: 422–428. [Medline] [CrossRef]
42. **Li C, Mizutani E, Ono T, Wakayama T.** An efficient method for generating transgenic mice using NaOH-treated spermatozoa. *Biol Reprod* 2010; **82**: 331–340. [Medline] [CrossRef]

Supplementary Text

Physiological characteristics of Pdx1-Venus Tg pigs

G1 offspring were obtained by breeding the founder Tg pigs with wild-type pigs. The weights of G1 Tg (one female and one male) offspring and a non-Tg (one male) littermate were assessed until the pigs were three months old. The postweaning blood glucose levels of these pigs were measured weekly until the same age. Blood samples collected from the ear vein were analyzed using a human blood glucose meter (Glucocard G+ meter, GT-1820; Arkray, Inc., Kyoto, Japan). At five months old, the fasting and postprandial blood insulin levels of the animals were measured.

Various aspects of blood biochemical parameters were analyzed in three G1 pigs aged between 5 and 15 months of age to determine whether the *Pdx1-Venus* Tg pigs had a normal physiology before and after sexual maturity. As a control, female and male non-Tg pigs, aged between 7 and 8 months of age, from the same litter as the Tg pigs were used. Blood urea nitrogen (BUN), glucose (GLU), creatinine (CRE), total protein (TP), total cholesterol (TCHO), triglyceride (TG), aspartate aminotransferase (AST), alanine aminotransferase (ALT), sodium (Na), potassium (K), and chloride (Cl) were measured using an auto analyzer (DRI-CHEM, FDC-700, Fujifilm, Tokyo, Japan). Insulin concentrations were measured using ELISA (Pig Insulin ELISA KIT (TMB), AKRIN-013T; Shibayagi, Gunma, Japan), and the concentrations of 1,5-anhydroglucitol (1,5-AG) were determined using the standard enzymatic method (SRL, Tokyo, Japan).

Suppl. Fig. 3 shows the physiological features of the Tg pigs and their non-Tg siblings. The G1 Tg piglets grew at the same rate as their non-Tg siblings (Suppl. Fig. 3A).

The non-fasting blood glucose levels of the Tg pigs, which were monitored consecutively after weaning until the pigs were 3 months old, were within the normal physiological range for blood glucose for pigs (Suppl. Fig. 3B). With regard to postprandial blood glucose and insulin levels, the Tg pigs showed similar reactions to those of non-Tg pigs (Suppl. Fig. 3C, D), indicating that the pancreatic functions of *Pdx1-Venus* Tg pigs were normal.

All 13 blood biochemical parameters measured were found to be within the normal ranges in the Tg pigs and their non-Tg control siblings (Suppl. Table 1). Blood 1,5-anhydroglucitol (1,5-AG) levels, indicators of glycemic control during the previous days, were also within the normal ranges in the Tg pigs.

A Conserved Rule for Pancreatic Islet Organization

Danh-Tai Hoang[1], Hitomi Matsunari[2], Masaki Nagaya[2], Hiroshi Nagashima[2], J. Michael Millis[3], Piotr Witkowski[3], Vipul Periwal[4], Manami Hara[5]*, Junghyo Jo[1,6]*

1 Asia Pacific Center for Theoretical Physics, Pohang, Korea, **2** Meiji University International Institute for Bio-Resource Research, Kanagawa, Japan, **3** Department of Surgery, The University of Chicago, Chicago, IL, United States of America, **4** Laboratory of Biological Modeling, NIDDK, NIH, Bethesda, MD, United States of America, **5** Department of Medicine, The University of Chicago, Chicago, IL, United States of America, **6** Department of Physics, POSTECH, Pohang, Korea

Abstract

Morphogenesis, spontaneous formation of organism structure, is essential for life. In the pancreas, endocrine α, β, and δ cells are clustered to form islets of Langerhans, the critical micro-organ for glucose homeostasis. The spatial organization of endocrine cells in islets looks different between species. Based on the three-dimensional positions of individual cells in islets, we computationally inferred the relative attractions between cell types, and found that the attractions between homotypic cells were slightly, but significantly, stronger than the attractions between heterotypic cells commonly in mouse, pig, and human islets. The difference between $\alpha - \beta$ cell attraction and $\beta - \beta$ cell attraction was minimal in human islets, maximizing the plasticity of islet structures. Our result suggests that although the cellular composition and attractions of pancreatic endocrine cells are quantitatively different between species, the physical mechanism of islet morphogenesis may be evolutionarily conserved.

Citation: Hoang D-T, Matsunari H, Nagaya M, Nagashima H, Millis JM, et al. (2014) A Conserved Rule for Pancreatic Islet Organization. PLoS ONE 9(10): e110384. doi:10.1371/journal.pone.0110384

Editor: Tao Cai, NIDCR/NIH, United States of America

Received July 9, 2014; **Accepted** September 12, 2014; **Published** October 28, 2014

Data Availability: The authors confirm that all data underlying the findings are fully available without restriction. All relevant data are within the paper and its Supporting Information files.

Funding: This research was supported in part by Basic Science Research Program through the National Foundation of Korea funded by the Ministry of Science, ICT & Future Planning (No. 2013R1A1A1006655) and by the Max Planck Society, the Korea Ministry of Education, Science and Technology, Gyeongsangbuk-Do and Pohang City (J.J.), the Intramural Research Program of the NIH, the National Institute of Diabetes and Digestive and Kidney Diseases (V.P.), and DK-020595 to the University of Chicago Diabetes Research and Training Center (Animal Models Core), DK-072473, AG-042151, and a gift from the Kovler Family Foundation (M.H.). The funders had no role in study design, data collection and analysis, decision to publish, or preparation of the manuscript.

Competing Interests: The authors have declared that no competing interests exist.

* Email: mhara@uchicago.edu (MH); jojunghyo@apctp.org (JJ)

Introduction

Multi-cellular organisms require communications between neighboring cells, and have developed special architectures for optimizing such cellular communications. A fundamental question in life is how organisms spontaneously form their functional structures. Interestingly, a few simple rules can be sufficient to form complex organs such as the lung [1]. As a microscopic explanation of morphogenesis, Steinberg introduced the *differential adhesion hypothesis* that differences in adhesiveness between cell types are partially responsible for the development and maintenance of organ structures [2,3].

Pancreatic islets of Langerhans are the critical micro-organs responsible for glucose homeostasis. Each islet consists mainly of α, β, and δ cells. Glucagon and insulin are the reciprocal hormones for increasing and decreasing blood glucose levels, secreted by α and β cells, respectively. The role of δ cells in glucose homeostasis is still mysterious. In addition, it has long been reported that endocrine cells interact with each other [4]. Considering the specific symmetries of interactions between α, β, and δ cells, their spatial organization must have functional significance. Rodent islets have a shell-core structure where β cells are located in the islet core, while non-β cells are located on the islet periphery. However, there are contradictory reports regarding the structure of human islets [5]. Some observations suggest more or less random structures of cells [6,7], while others have found some order in structures, and described human islets as assemblages of β-cell-core subunits [8] or lobules [9], cloverleaf patterns [5], ribbon-like structures [10], and folded trilaminar plate [11].

Dissociated islet cells spontaneously aggregate and form islet-like structures, *pseudo-islets*, in rat, pig, and human pancreatic cultures [12–15]. Different adhesion molecules have been proposed as a cause of the pseudo-islet formation expressed on rodent α and β cells [16–20]. However, the relative adhesion strengths of such cells in native islets has not been directly measured. On one hand, this technical limitation leaves open the interesting question of whether different species have different rules for islet organization. On the other hand, current imaging methods allow to observe islet structures with high resolution. In this study, we computationally infer the organization rule from three-dimensional islet structures. In particular, we compare mouse, pig, and human islets, and find a conserved organization rule behind different islet structures.

Results

Cellular distributions in pancreatic islets

Two-dimensional cross sections of pancreatic islets have been widely used to study islet structures. Here, however, we used a confocal microscope to examine three-dimensional islet structures, as previously used [6,21]. To precisely analyze islet structures, we obtained three-dimensional positions of every endocrine cell in

individual islets. We used stained nuclei to determine the center positions of cells, and immunostaining to determine cell types. Figure 1 showed the spatial cellular organizations of pancreatic islets in different species. First, we observed two major cell types of α and β cells in mouse (Fig. 1*A*), pig (Fig. 1*B*), and human islets (Fig. 1*C*). Mouse islets showed the typical shell-core structure in which β cells are located in the core, while α cells are located on the periphery. In pig and human islets, however, α cells are located not only on the periphery but also distributed inside islets.

We then quantified the fraction of β cells depending on islet size in the three species (Fig. 2). Mouse islets consisted of 90% β cells independent of islet size. Human islets had a smaller β-cell fraction, P_β. In particular, larger human islets had less abundant β cells depending on size. This finding in three-dimensional islets is consistent with previous reports based on pancreatic sections [11,22,23]. Interestingly, pig islets ($P_\beta = 0.87-0.91$) showed an intermediate characteristic between mouse ($0.91-0.94$) and human islets ($0.62-0.78$). We also examined cell-to-cell contacts (See Materials and Methods), and quantified their ratios, $P_{\alpha\alpha}$, $P_{\beta\beta}$, and $P_{\alpha\beta}$ for $\alpha-\alpha$, $\beta-\beta$, and $\alpha-\beta$ contacts, respectively (Fig. 3). The higher β-cell fraction in mouse islets resulted in more prevalent $\beta-\beta$ contacts ($P_{\beta\beta} = 0.89-0.91$), compared with pig ($0.78-0.85$) and human islets ($0.46-0.64$), but less prevalent $\alpha-\alpha$ and $\alpha-\beta$ contacts.

Given fractions of α and β cells, we could simulate cell-to-cell contact probabilities in random cell aggregates. The probability that two sites are occupied randomly by α cells is $P_{\alpha\alpha} = P_\alpha^2$, and the one for β cells is $P_{\beta\beta} = P_\beta^2$. In addition, the probability that two sites are occupied randomly by α and β, or vice versa, is $P_{\alpha\beta} = P_\alpha P_\beta + P_\beta P_\alpha = 2P_\alpha P_\beta$. Regardless of species, Fig. 3 shows that frequencies of homotypic contacts are significantly higher than the probabilities in random aggregates ($P_{\alpha\alpha} > P_\alpha^2$ and $P_{\beta\beta} > P_\beta^2$). On the other hand, islet structures showed smaller frequencies of heterotypic contacts, compared with random ($P_{\alpha\beta} < 2P_\alpha P_\beta$). These results clearly demonstrated that islet structures are not random cell aggregates. This conclusion looks trivial for the shell-core structure of mouse islets (Fig. 1*A*). However, this suggested that pig and human islets also had some order in their cellular organization.

Self-organization rule for pancreatic islets

Since islets are not random cell aggregates, we investigated rules governing islet structure. Prevalent contacts of homotypic cells could have resulted from (i) replication of neighboring cells and/or (ii) stronger attraction between homotypic cells. Islet organogenesis occurs in the milieu of developmental processes including cell differentiation, migration, aggregation, replication, and death [24,25]. Nevertheless, when islet cells are dissociated, they can spontaneously form pseudo-islets resembling native islets [12–15]. This pseudo-islet formation implies that sequences of complicated developmental processes, particularly cell replication, may not be critical for the formation of equilibrium islet structures. Therefore, as proposed [2,3,26], we investigated if the differential adhesion hypothesis could provide a simple rule governing for islet structures. Depending on the relative adhesiveness between cell types, islets could have various equilibrium structures (Fig. 4). When homotypic attractions are stronger than heterotypic attractions, islets have a sorting phase with two homogeneous cell

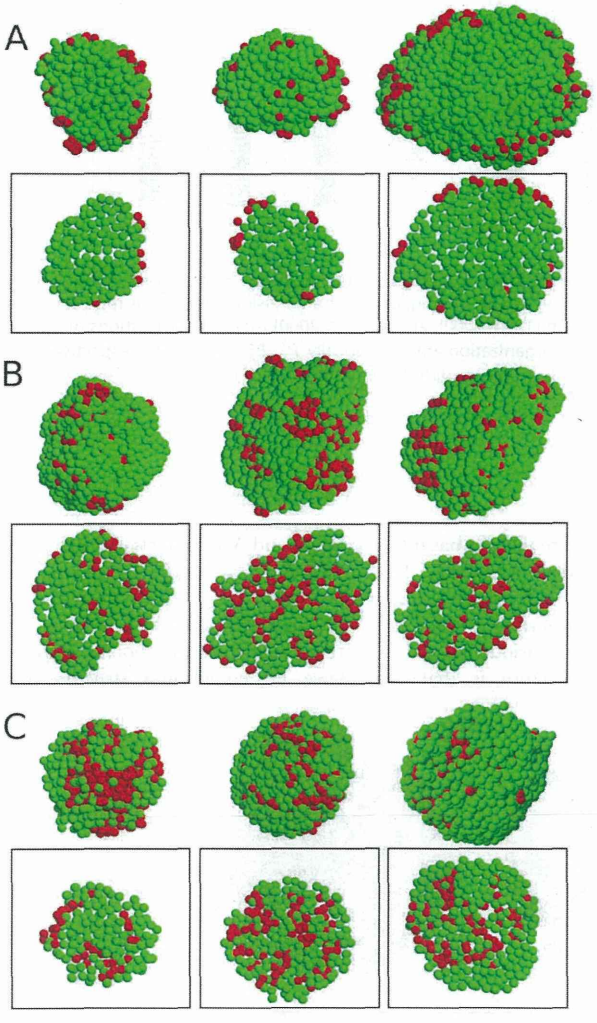

Figure 1. Cellular organization of pancreatic islets. Three-dimensional spatial distribution of α cells (red) and β cells (green) is shown in (*A*) mouse, (*B*) pig, and (C) human islets. To show internal islet structures clearly, their corresponding two-dimensional sections are also shown in boxes.
doi:10.1371/journal.pone.0110384.g001

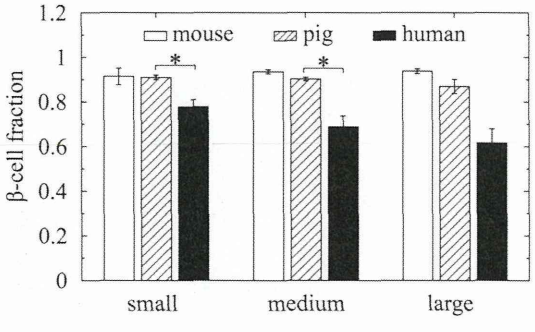

Figure 2. Cellular compositions in mouse, pig, and human islets. Fractions of β cells, depending on islets size, are calculated in mouse (empty bar), pig (hatched), and human (black solid) islets. Islet size is represented by the total number of cells in islets, and categorized as small (<1000 cells), medium (1000–2000), and large (>2000) islets. Mean ± SEM (n = 30). $^*P<0.005$.
doi:10.1371/journal.pone.0110384.g002

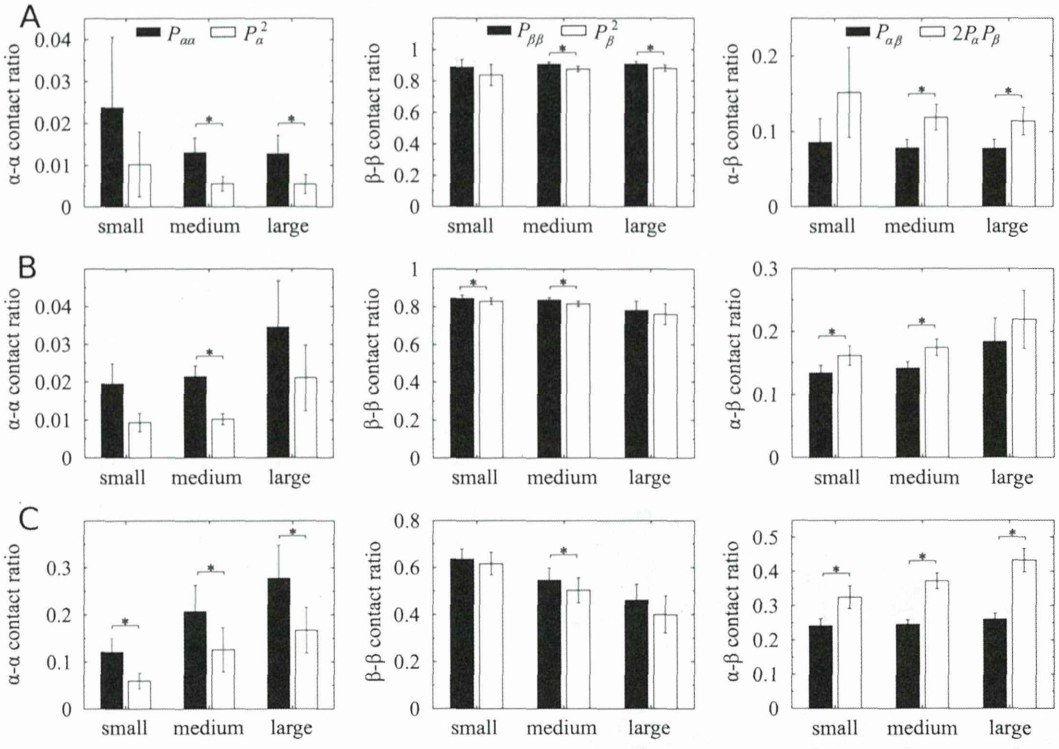

Figure 3. Cell-to-cell contact ratios in mouse, pig, and human islets. Based on the contacts between neighboring cells, ratios of $\alpha-\alpha$, $\beta-\beta$, and $\alpha-\beta$ contacts ($P_{\alpha\alpha}$, $P_{\beta\beta}$, and $P_{\alpha\beta}$), depending on islet size, are calculated in (*A*) mouse, (*B*) pig, and (*C*) human islets. Islet size is represented by the total number of cells in islets, and categorized as small (<1000 cells), medium (1000–2000), and large (>2000) islets. Given fractions of α and β cells (P_α and P_β), the $\alpha-\alpha$, $\beta-\beta$, and $\alpha-\beta$ contact probabilities in random cell organization are theoretically P_α^2, P_β^2, and $2P_\alpha P_\beta$, respectively. The random organization (empty bar) is compared with the organization of native islets (black solid). Mean ± SEM. $^*P<0.005$.
doi:10.1371/journal.pone.0110384.g003

clusters. As heterotypic attraction becomes stronger, the two cell types start to mix [27].

We specify the relative strengths of adhesiveness or attraction between cell types as $J_{\alpha\alpha}$, $J_{\beta\beta}$, and $J_{\alpha\beta}$ for $\alpha-\alpha$, $\beta-\beta$, and $\alpha-\beta$ contacts, respectively. A stronger attraction between neighboring cells implies that it requires a larger amount of energy to dissociate them. Therefore, the total cell-to-cell contact energy, *self-energy*, in an islet is a sum over every contact

$$E=-J_{\alpha\alpha}N_{\alpha\alpha}-J_{\beta\beta}N_{\beta\beta}-J_{\alpha\beta}N_{\alpha\beta}, \quad (1)$$

where the islet has total $N_{\alpha\alpha}$, $N_{\beta\beta}$, and $N_{\alpha\beta}$ contacts of $\alpha-\alpha$, $\beta-\beta$, and $\alpha-\beta$, respectively. The negative sign in Eq. (1) represents that external energy is needed (not extracted) to dissociate cell-to-cell contacts. Given numbers of α and β cells, the islet self-energy can have various values depending on spatial organization of cells. Our conjecture is that islets have an equilibrium structure that

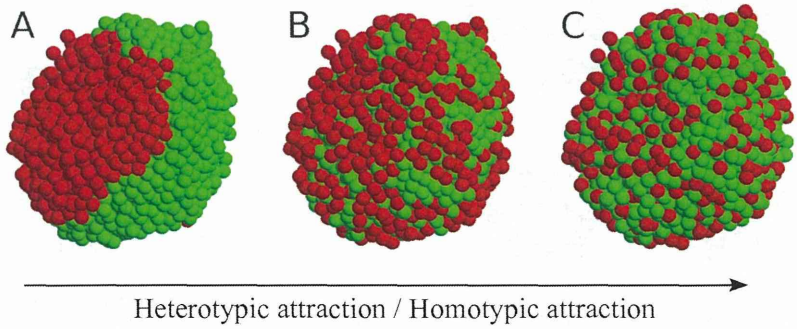

Figure 4. Schematic diagram of structural dependence on relative attractions between cell types. A sorting structure of two cell types is changed to mixing structures, as heterotypic attraction increased compared with homotypic attractions: (*A*) complete sorting, (*B*) shell-core sorting, and (*C*) mixing structures.
doi:10.1371/journal.pone.0110384.g004

minimizes their self-energy. When homotypic attractions are stronger, $\alpha-\alpha$ and $\beta-\beta$ contacts are preferred. On the other hand, when heterotypic attraction is stronger, $\alpha-\beta$ contacts are preferred.

Here our problem is not to obtain equilibrium structures given cellular attractions. It is currently not possible to measure the strengths of cellular attractions inside islets. However, we could obtain cell-to-cell contact information from three-dimensional islet imaging. Thus we addressed this inverse problem to infer the strengths of cellular attractions from cell-to-cell contact information. Using Bayesian inference (See Materials and Methods), we inferred the likelihood strengths of cellular attractions that explain observed islet structures. Figure 5 showed the inferred attractions, $J_{\beta\beta}$ and $J_{\alpha\beta}$, relative to the reference attraction $J_{\alpha\alpha}=1$, from mouse, pig, and human islets. The relative attractions were not dependent on islet size for all species (Fig. S1). Their averages and standard deviations are summarized in Table 1. The relative attractions were not dramatically different between each other, regardless of species. The homotypic attractions, $J_{\alpha\alpha}$ and $J_{\beta\beta}$, were slightly, but significantly, larger than the heterotypic attraction, $J_{\alpha\beta}$, for all species considered. This general conclusion is consistent with the cellular organization, $P_{\alpha\alpha}>P_{\alpha}^2$, $P_{\beta\beta}>P_{\beta}^2$, and $P_{\alpha\beta}<2P_{\alpha}P_{\beta}$. A random organization can be obtained with equal cellular attractions, i.e., $J_{\alpha\alpha}=J_{\beta\beta}=J_{\alpha\beta}$. It is thus understandable that islets have $J_{\alpha\beta}<J_{\alpha\alpha}$ and $J_{\beta\beta}$. However, the Bayesian inference quantified the dependence of relative cellular attractions on species: $J_{\alpha\beta}/J_{\beta\beta}$ for mouse islets (0.91) is lowest, while human islets (0.98 and 0.99 for two different pancreata) show the largest ratio. Pig islets showed a similar ratio (0.97) to human islets.

Here, an intriguing question is whether the small differences in cellular attractions can explain the structural difference between mouse and human islets. In general, binary mixture systems of finite size can generate sorting and mixing phases depending on mixture fraction and relative adhesion strengths [27]. To answer the question, we considered two theoretical lattices representing

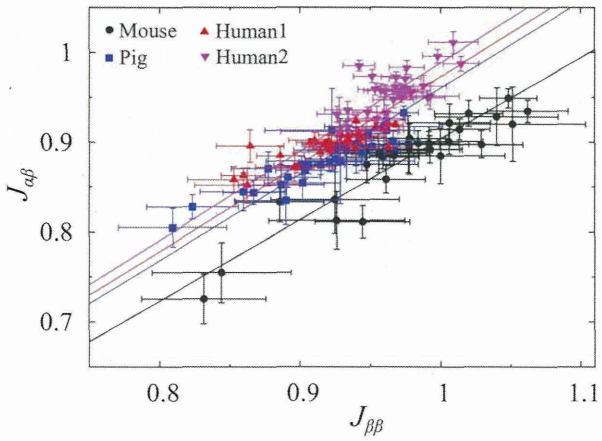

Figure 5. Cellular attractions in mouse, pig, and human islets. Relative attractions between cell types and their uncertainties are inferred from three-dimensional islet structures. Symbols represent individual islets: mouse (black circle), pig (blue square), and human islets (red triangle and pink inverse triangle). Each species has n = 30 islets. In particular, two sets of n = 30 islets are provided from two human (Human1 and Human2) subjects. The relationship between $J_{\alpha\beta}$ and $J_{\beta\beta}$ is fitted with linear functions, $y=ax$, represented by solid lines with colors corresponding to each species. Note that the attraction between α cells is defined as a reference attraction, $J_{\alpha\alpha}=1$.
doi:10.1371/journal.pone.0110384.g005

islet structures: cubic (Fig. 6*A*) and hexagonal close packed (HCP) lattices (Fig. 6*B*), in which α and β cells are distributed with various β-cell fractions P_{β} and relative attraction strengths $J_{\alpha\beta}/J_{\beta\beta}$. Then we computed cell-to-cell contact numbers and their fluctuations, and obtained the phase diagrams for the cubic lattice (Fig. 7*A*) and the HCP lattice (Fig. 7*B*). Human and pig islets were classified to have the partial mixing structure for both cubic and HCP lattices. However, mouse islets were classified to have the partial mixing structure for the cubic lattice, but to have the shell-core sorting structure for the HCP lattice. The native islet structure could be approximated better as the HCP lattice than the cubic lattice, because its mean number of neighboring cells (8.6 ± 0.3 for mouse, 8.5 ± 0.3 for pig, 8.4 ± 0.3 for Human1, and 8.3 ± 0.6 for Human2 islets) was closer to the HCP lattice (10.6) than the cubic lattice (5.4). Therefore, we concluded that the higher β-cell fraction P_{β} and the slightly weaker heterotypic attraction $J_{\alpha\beta}/J_{\beta\beta}$ of mouse islets could be sufficient to generate the shell-core sorting structure, distinct from the partial mixing structure of human and pig islets.

Spatial organization of δ cells

In addition to α and β cells, islets contain a minor population of somatostatin-secreting δ cells. We further examined human islet structures including δ cells (Fig. 8). Similarly to previous analysis, we inferred cellular attractions, relative to $\alpha-\alpha$ attraction ($J_{\alpha\alpha}=1$), not only $J_{\beta\beta}$ and $J_{\alpha\beta}$, but also $J_{\delta\delta}$, $J_{\alpha\delta}$, and $J_{\beta\delta}$ (Table 2). The result could be summarized as $J_{\alpha\alpha}\approx J_{\beta\beta}\approx J_{\delta\delta}>J_{\alpha\beta}\approx J_{\alpha\delta}\approx J_{\beta\delta}$. In general, homotypic attractions were slightly stronger than heterotypic attractions.

To validate our previous analysis with islets in which δ cells are unseen, we inferred $J_{\beta\beta}$ and $J_{\alpha\beta}$ from islets in which δ cells are seen, but ignored as empty sites. Their inferred values were not different regardless of the presence and absence of δ cells (Table 2).

Discussion

We observed spatial distributions of endocrine cells in three-dimensional islets, and characterized their distributions in mouse, pig, and human islets. Islets from different species showed different cellular compositions and structures. An intriguing question was whether the structural difference originates from the different cellular composition or different organization rules, or both. Based on our computational inference from the high-resolution islet structures, we found that the adhesions between homotypic cells were slightly, but signficantly, stronger than the ones between heterotypic cells commonly in the three species. Furthermore, the binary mixture simulation on the HCP lattice demonstrated that the small difference of relative adhesions and the more abundant β cells could generate the shell-core structure of mouse islets, which was different from the partial mixing structure of pig and human islets. Therefore, the conserved rule could explain the different islet organizations of the three species.

We considered islet organogenesis as an equilibrium process assuming that given numbers of cells can switch their positions and minimize their total contact energy, the islet self-energy. One might consider it as a non-equilibrium process where the sequential events of cell differentiation and replication elaborately construct the specific structures of islets during development. However, sequential development is limited to explain the following two observations. First, cell replication could explain the preferential neighboring of homotypic cells, but it could not explain the regional segregation of α cells and β cells in mouse islets without extra processes such as cell polarization, migration,

Table 1. Cellular attractions in mouse, pig, and human islets.

Species	n	$J_{\beta\beta}$	$J_{\alpha\beta}$	$J_{\alpha\beta}/J_{\beta\beta}$
Mouse	30	0.97±0.05	0.88±0.05[a]	0.91±0.02
Pig	30	0.91±0.04	0.88±0.03[a]	0.97±0.02[b]
Human1	30	0.92±0.03	0.90±0.02[a]	0.98±0.02
Human2	30	0.97±0.02	0.96±0.02[a]	0.99±0.02

Relative attractions between cell types are inferred from three-dimensional islet structures, mean ± SD (n = 30 islets). Note that the attraction between α cells is defined as a reference attraction, $J_{\alpha\alpha}=1$.

[a]Paired Student's t-test concludes $J_{\beta\beta}>J_{\alpha\beta}$ with $P<0.005$.

[b]Unpaired Student's t-test concludes that mouse and pig islets have different $J_{\alpha\beta}/J_{\beta\beta}$ with $P<0.005$.

doi:10.1371/journal.pone.0110384.t001

and death. In contrast, the equilibrium process, based on the differential adhesion hypothesis, may provide a simpler explanation for the regional segregation problem. Second, when endocrine cells are dissociated from mature islets, they can re-aggregate and form pseudo-islets resembling the native islets [12–15]. The pseudo-islet formation gives direct evidence suggesting that the sequence of developmental events might not be critical for the determination of islet structures. Assuming that cellular motility is sufficiently large, the detailed history of cell additions through differentiation and replication may not significantly affect the equilibrium islet structures.

Here we proposed a *dynamic structure* of islets, balancing cell motility and adhesion, instead of a static structure where cellular positions were frozen. Lymphocyte homing is an extreme example of a dynamic structure because highly mobile immune cells can organize lymphoid organs such as germinal centers and Peyer's patches through chemotoxis and adhesion [28,29]. In this study, we quantified the cellular attraction J_{xy} as a required energy to dissociate the contact of x and y cells, and represented the cell motility T as a kind of fluctuation energy to help the cellular contacts dissociate. As the cell motility T increased, cells could break their contacts to neighboring cells more frequently and move more actively. Our analysis showed that the the relative attractions between cell types were not dramatically different in pancreatic islets. Quantitatively, the energy gap between the relative cellular attractions did not exceed the fluctuation energy for cell motility to dissociate the cellular contacts, $J_{\beta\beta}-J_{\alpha\beta}<T$.

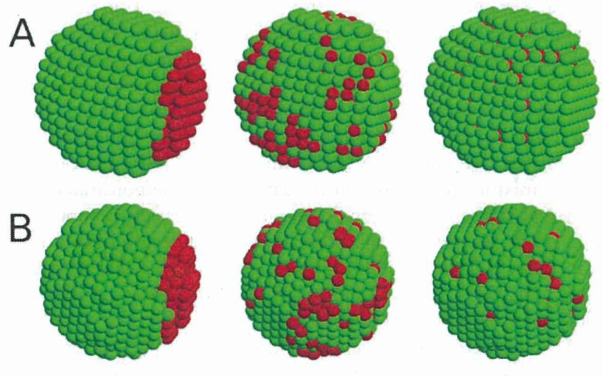

Figure 6. Distinct structures of binary mixtures. Complete sorting, shell-core sorting, and partial mixing structures are plotted for (*A*) cubic and (*B*) hexagonal close packed lattices. Here each lattice consists of 1357 cells with 10% α cells (red) and 90% β cells (green). The relative attractions are chosen to have the specific structures: $J_{\alpha\beta}=0.7$ (left), 0.85 (middle), and 1.1 (right) for (*A*) the cubic lattice; and $J_{\alpha\beta}=0.7$ (left), 0.93 (middle), and 1.1 (right) for (*B*) the hexagonal close packed lattice. Note that the homotypic attractions are fixed as a reference, $J_{\alpha\alpha}=J_{\beta\beta}=1$, and the thermal fluctuation energy is $T=0.2$.

doi:10.1371/journal.pone.0110384.g006

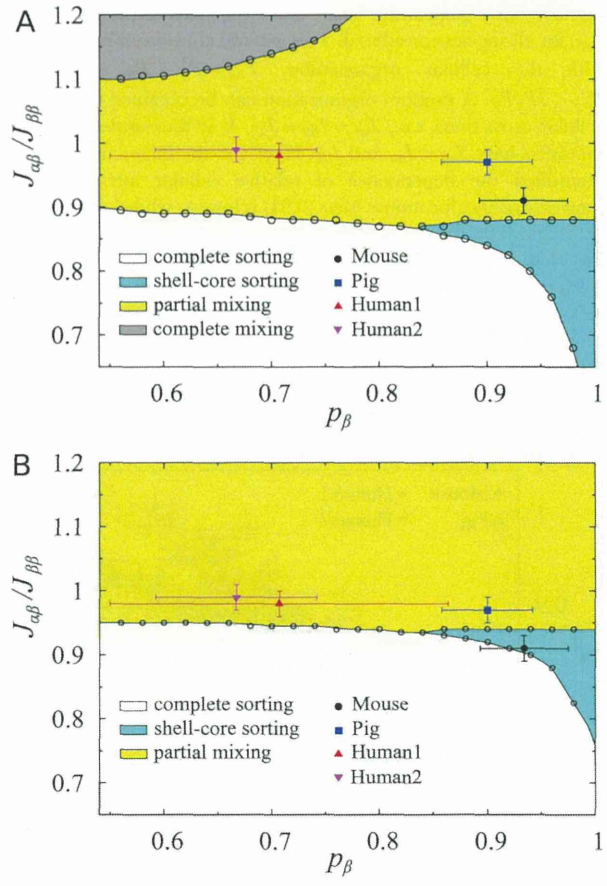

Figure 7. Phase diagrams of binary mixtures. Binary mixtures have complete sorting (white region), shell-core sorting (cyan region), partial mixing (yellow region), and complete sorting (gray region) structures depending on mixture fraction and relative adhesion strengths. Plotted are phase diagrams for (A) cubic and (B) hexagonal close packed lattices with 1357 cells. Symbols represent the observed β-cell fraction P_β and the inferred relative attraction $J_{\alpha\beta}/J_{\beta\beta}$ of mouse islets (black circle), pig (blue square), and human islets (red triangle and pink inverse triangle). Note that the homotypic attractions have a reference attraction, $J_{\alpha\alpha}=J_{\beta\beta}=1$. Each species has n = 30 islets. Mean ± SD.

doi:10.1371/journal.pone.0110384.g007